Check for updates

Metal oxide nanomaterial-based sensors for monitoring environmental NO$_2$ and its impact on the plant ecosystem: a review

Shrestha Tyagi, [iD] Manika Chaudhary, Anit K. Ambedkar, Kavita Sharma, [iD] *
Yogendra K. Gautam and Beer Pal Singh [iD] *

The substantial increase in the emission of air pollutants due to the rapid industrial growth, combustion of fossil fuels, pesticides, and insecticides used in the agriculture sector in the last few decades urgently requires sincere remedial efforts from the global scientific community. The elevated concentration of nitrogen dioxide (NO$_2$) makes it one of the most common and catastrophic air pollutants. NO$_2$ acts as a precursor for ozone (O$_3$) and particulate matter (PM) and participates in the phenomena of acidification and eutrophication in plant ecosystems. Therefore, worldwide research is ongoing towards designing an accurate, reliable, and environment-friendly NO$_2$ gas detection technology for the monitoring of NO$_2$ concentration in the earth's environment. Nanostructured metal oxide semiconductors (NMOSs) have been found to be very consistent and precise for NO$_2$ sensing due to their outstanding structural and morphological properties. The first part of this review presents an overview of the effects of NO$_2$ pollution on the plant ecosystem. The second part briefly describes the various other available techniques for NO$_2$ detection. Further, this article presents a comprehensive review on the progress of a wide variety of NMOS-based NO$_2$ gas sensors. NMOS materials with diverse morphologies such as nanorods, nanoparticles, nanowires, nano flowers, and nanosheets, fabricated into NO$_2$ gas sensors, are discussed extensively. Moreover, their fabrication methods and performance in terms of sensitivity/selectivity, operating temperature, response/recovery time, and detection limit, along with their gas sensing mechanism, are explained in the review in order to establish a reliable NO$_2$ gas detection technology.

1. Introduction

Air pollution is an immense concern worldwide in recent times and can cause ruthless problems for human health as well as for the ecosystem. According to the World Health Organization (WHO), with atmospheric concentrations of NO$_2$ higher than 30 μg m^{-3} on a 24 hour yearly average and 95 μg m^{-3} on a 4 hour average, NO$_2$ is considered as the chief air pollutant.[1] The burning of fossil fuels and emissions from vehicles and industries are the main sources of excess NO$_2$ in ambient air.[2] NO$_2$ can now produce ground level or "bad" ozone multiple times, which in turn is a potent greenhouse gas and air pollutant.[3] This ground-level ozone may penetrate the stomata of plants, causing them to close, thus preventing CO$_2$ transport, and ultimately ensuing the reduction of the photosynthesis process.[4] Excess NO$_2$ not only poses a threat to living organisms but also accounts for serious impacts on the environment *via* acid rain, eutrophication, the greenhouse

effect, global warming, and climate change. Fig. 1 depicts the various natural and anthropogenic sources of NO$_2$ emissions and the effects of high concentrations of NO$_2$ on foliar physiology, plant metabolism, leaf nutrition, and the mechanism of plant growth.

In view of the above information, sincere and effective efforts are required for the accurate detection of NO$_2$ concentrations in the ecosystem. Several techniques are available for the monitoring of nitrogen dioxide; however, only a few can be applied to measure NO$_2$ at concentrations below parts per billion (ppb). These techniques of NO$_2$ detection are mainly based on the surface conversion techniques in which NO$_2$ is first converted to NO, which is subsequently detected by chemiluminescence technique. Other NO$_2$ detection techniques include optical,[5] photoacoustic,[6] gas chromatographic methods,[7] and nanostructured metal oxide semiconductor (NMOS)-based gas sensors.[8] NMOS gas sensors are one of the emerging technologies among the various NO$_2$ sensing techniques.[9] The NMOS gas sensors have many advantages in comparison to other available gas sensors[10,11] in terms of their abundance, cost-effectiveness, ease of fabrication, small size,

Smart Materials and Sensor Laboratory, Department of Physics, Chaudhary Charan Singh University, Meerut, U.P, 250004, India.
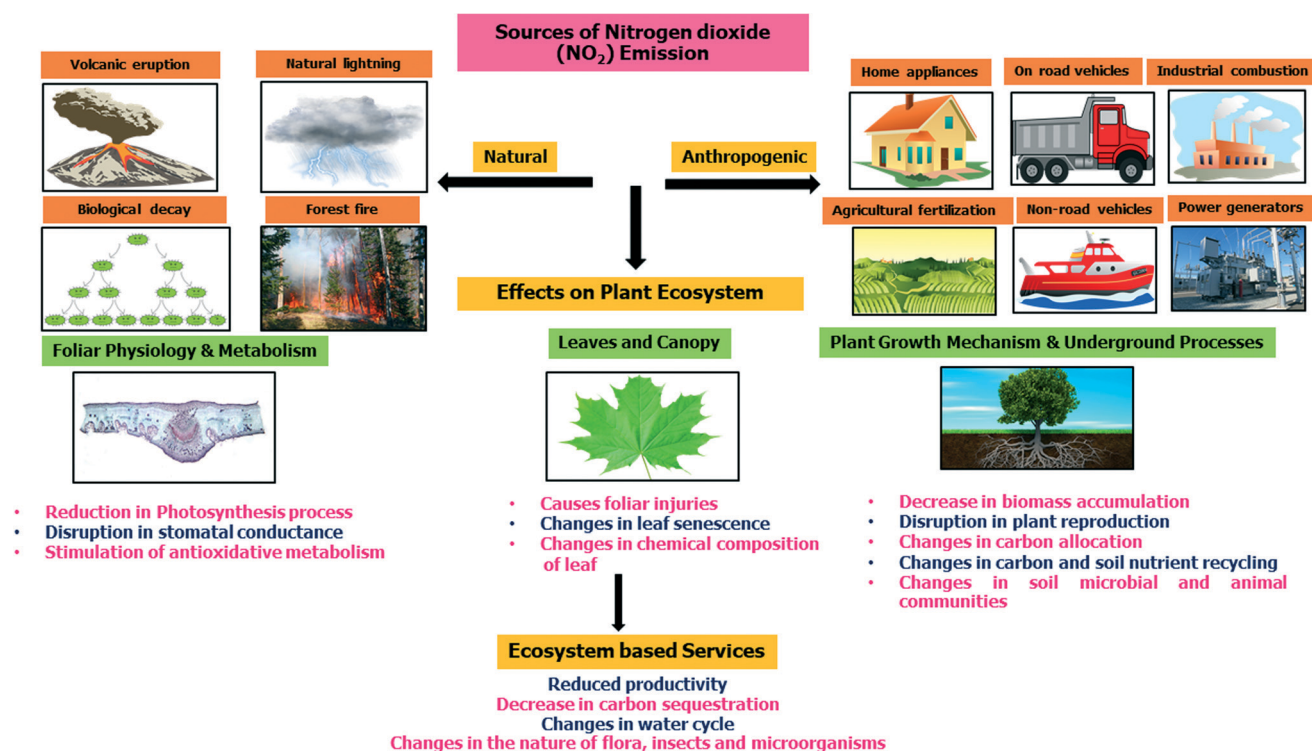*E-mail: sharmak29@gmail.com, drbeerpal@gmail.com*

Fig. 1 Schematic diagram of the sources of NO_2 pollution and their effects on plant ecosystems.

simple integration in electronics, easy maintenance, as well as moderate stability and safety.[12] The NMOS materials possess a wide band gap, which allows them to have a full spectrum of electronic properties.[9] Gas sensors based on wide band gap MOS are suitable due to their reversible and big changes in the electrical resistance, along with the excellent thermal, chemical, environmental, and radiation stability and mechanical robustness.[13] The properties of the NMOS sensors are dependent on the material's size[14] and its microstructure.[15] The small grain size of the material provides a more specific area, which allows more oxygen ions and NO_2 molecules to adsorb on the surface of the material. The various studies on the particle size and micro-structural dependent sensing property of the NMOS-based sensors are given in the following sections of the article. There are many fabrication processes to obtain NMOS materials with diversifying microstructures and morphologies. Sensing materials with specific morphologies can be synthesized using hydrothermal and sol–gel methods. Meanwhile, different techniques, including physical vapor deposition (PVD), epitaxial growth, chemical vapor deposition (CVD) and thermal spray, were used for the fabrication of thin films as sensing layers having controlled thickness.[16] In addition, there are plenty of methods, including doping, organic sensitization, inorganic heterojunction sensitization, and oxygen vacancy modification, that can be used to improve the NO_2 sensing performance of NMOS sensors.[17] These methods

govern the type of reaction and rate of gases at the surface of the sensor, and demonstrate a significant effect on the sensitivity, response time, recovery time, and selectivity of the sensors.[18] The NMOS gas sensors require high temperature to operate. Currently, various efforts have been made for NMOS sensors that can operate at room temperature for monitoring NO_2. Thus, NMOS gas sensors are nowadays progressing in the direction of low operating temperature, simple integration, and low energy consumption. In spite of some complications of the operating temperature, NMOS sensors are still an appealing technology for measuring NO_2.

The main objective of this review article is to comprehensively study the NMOS-based NO_2 gas sensors in order to establish a strong detection technique for the NO_2 concentrations. This review also elaborates on the effects of elevated levels of air pollutant 'NO_2' on the plant ecosystem. Specifically, the mechanism of plant growth in the excess NO_2 environment is discussed in the following section. A wide variety of NMOS (ZnO, SnO_2, In_2O_3, TiO_2, WO_3, CuO, NiO, and Co_3O_4)-based NO_2 gas sensors are studied, along with their gas sensing mechanism. The recent major developments in NMOS-based NO_2 gas sensors are also reviewed. Moreover, gas sensing parameters of primary interest, such as gas response time/sensitivity, recovery time, selectivity, and the detection limit of MOS nanomaterials for NO_2 gas sensing, are discussed in detail. Furthermore, this

review article highlights the performance of NMOS-based NO_2 gas sensors over the various other available NO_2 sensing techniques.

2. Effects of NO_2 on the plant ecosystem

Plants play an important role in the construction of the ecological environment by decomposing and absorbing harmful gases. The amount of biologically active nitrogen compounds has risen dramatically as a result of human activities, both industrial and agricultural, disrupting the natural nitrogen cycle. Nitrogen in several forms, primarily NO_x (NO, NO_2) and NH_3 as dry deposition, and NO_3 and NH_4 as wet deposition, pollutes the air. NO_2 can also be converted to nitrates, which can cause fine particle pollution as a secondary pollutant.[1] It acts as a precursor for harmful secondary air pollutants, mainly ozone and particulate matter. Nitrogen dioxide contributes to ground-level ozone through a complex sequence of chemical reactions that take place in the sunlight. NO_2 levels above a certain threshold can harm vegetation, causing leaf damage and reduced growth. It increases the susceptibility of plants to disease and frost damage. In the presence of sunlight, NO_2 reacts with other air pollutants and forms ozone, which can damage plants at high concentrations. An excessive amount of nitrogen dioxide in the atmosphere can damage plants, harm the leaves, and reduce the growth and yield of many crops.[4] High NO_2 concentration levels have potentially toxic effects on plants, such as acid rains, which lowers the pH of water and soil. This gives rise to harmful effects, and even death of plants and biological systems. Presently, researchers hold different opinions towards the effects of NO_2 on plants. NO_2 can form organic nitrogenous compounds in the plants after being metabolized and incorporated into the nitrate assimilation pathway.[21] However, most plants have low NO_2–N penetration into total plant nitrogen, as well as resistance towards NO_2. Exposure of plants towards NO_2 causes a variety of physiological responses, including changes in the antioxidant enzyme activity,[22] nitrogen metabolic enzyme activity, and dispersal of nitrogenous metabolic products in plant tissues. Low concentrations of NO_2 in the water lead to the formation of nitrate and nitrite, which are further used by plants during the normal phase of nitrate metabolism; therefore, NO_2 may be used as an airborne fertilizer.[23] High NO_2 concentrations, on the other hand, may cause excessive accumulations of nitrite and acidification of cells.[24,25] It shows negative responses in plants, such as the development of reactive oxygen species (ROS). In addition, the reduction of nitrogen assimilation and plant growth with severe leaf damage, chlorosis in the plant, or even plant death, can happen. However, different plant organisms have different physiological responses towards NO_2. Therefore, the effects of NO_2 on plant ecosystems are still passionately debated, and no consensus has been achieved.

The corrosive and oxidative properties of NO_2 are the primary reason for plant injury that affects various biochemical and physiological processes after entering through the stomata of plant leaves. Several stomatal characteristics, such as dimensions and stomatal conductance, cuticular chemical compositions, and environmental factors, affect the foliar NO_2 uptake. The plant growth is reduced by NO_2 and the damage suffered by the plant is based on various factors, including the length of exposure, age of the plant, humidity conditions, light and edaphic factors.[26] Recently, Sheng et al.[28] explored the physiological and biochemical responses of two precious species, *Carpinus betulus* and *Carpinus putoensis*, for a high concentration of NO_2 stress and their recovery. The seedlings of the two species underwent fumigation with 12.0 mg m^{-3} NO_2 for 0, 1, 6, 12, 24, 48, and 72 h. In terms of peroxidase (POD) activity, the damage response of *C. betulus* under NO_2 stress appeared later than that of *C. putoensis*. *C. putoensis* exhibited more sensitive metabolisms towards NO_2 stress as compared to *C. betulus*. After stress removal, both *Carpinus* species recovered to normal growth through their metabolism after 30 days.[27] The leaf injury symptoms of both *Carnipus* species towards NO_2 exposure and after recovery, along with the fumigation test device setup, are shown in Fig. 2.

Sheng et al.[28] investigated the effects of NO_2 on biochemical responses in 41 garden plants by exposing all of the plants towards 6 μL L^{-1} NO_2 in an open-top glass chamber. Measurements of the various physiological parameters, such as chlorophyll content (Chl), peroxidase (POD) activity, along with malondialdehyde (MDA) concentrations, and leaf mineral ion contents nitrogen, phosphorus, potassium, calcium, magnesium, and zinc of all 41 garden plants were carried out. The results reveal that NO_2 damages the plants and influences the Chl content in the leaf in most of the functional groups. Changes in mineral ion concentrations, as well as increases in POD activity and soluble protein and MDA concentrations, may serve as signals for inducing defense responses.[28] Chen et al. reported the effect of NO_2 fumigation oxidative stress and antioxidative response in *Cinnamomum camphora* seedlings at low-volume fractions for 60 days and demonstrated that 4.0 μL L^{-1} of NO_2 exposure significantly reduced the Chl content in the leaves of *Cinnamomum camphora* seedlings. The change in the Chl content was responsible for changes in the leaf color that resulted in yellow spots or yellow leaves.[29] Hu et al. used a photosynthesis method and a scanning electron microscope to examine the effects of gaseous NO_2 on stomatal conductance, photosynthesis, dark- and photorespiration in *Populus alba × Populus berolinensis* hybrid leaves. The results indicated that after 14 and 48 hours of exposure towards 4 μL L^{-1} of NO_2, the net photosynthesis of *Populus alba × Populus berolinensis* hybrid leaves decreased significantly, demonstrating that photosynthesis inhibition may be the reason for NO_2 growth suppression.[30] Sheng et al.[31] reported leaf physicochemical responses, stomatal
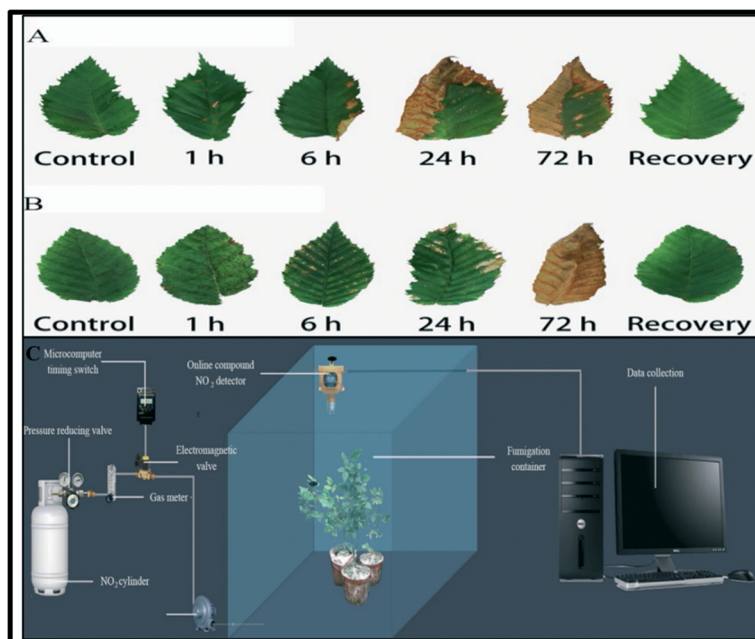
Fig. 2 Leaves of (A) *Carpinus betulus* (B) and *Carpinus putoens* showing injury symptoms under different NO_2 exposure times and after natural recovery. (c) The experimental set-up for timing regulation and recording of NO_2 concentration.[27]

characteristics, and chloroplast structure of *Carpinus putoensis* W. C. Cheng after exposure to 6 μL L^{-1} NO_2 for periods 0, 1, 6, 24, and 72 h and natural recovery of 30 days. The short-duration exposure towards a high concentration of NO_2 had major negative impacts ($p < 0.05$) on the Chl content, photosynthesis, and chloroplast-related physicochemical processes of *C. putoensis* leaves, except for one hour of NO_2 exposure, which was proven to be beneficial

for the physiological responses of plant. Furthermore, exposure of NO_2 formed swelling of the thylakoids inside the chloroplasts and increased the thickness of the palisade/spongy tissue. This thylakoid swelling could be reduced by the removal of the pollutant from the air flow. Scanning electron microscopy (SEM) images, along with diurnal changes such as net photosynthesis (P_n), stomatal conductance (G_s), transpiration rate (T_r) and intercellular CO_2
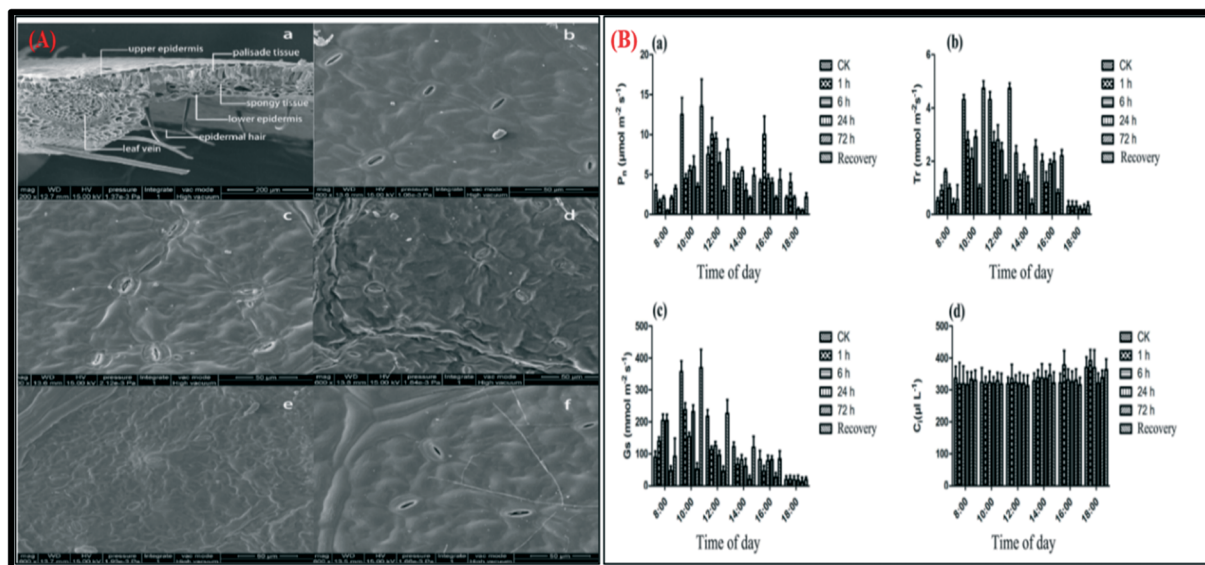

Fig. 3 (A) (a) SEM images of a leaf cross-section, (b) leaf stomata in the control group, (c–e) NO_2-treated groups exposed to 6 μL L^{-1} NO_2 for 1, 24 and 72 h, respectively, and (f) the post-recovery group. (B) The diurnal changes (bar graphs form) in photosynthesis in *C. putoensis* leaves grown with exposure to 6 μL L^{-1} NO_2 for 0, 1, 6, 24, and 72 h after a recovery period; (a) net photosynthesis (P_n), (b) stomatal conductance (G_s), (c) transpiration rate (T_r) and (d) intercellular CO_2 concentration (C_i).[31]

concentration (C_i) of *C. putoensis* leaves in the form of bar graphs with exposure to 6 μL L^{-1} NO$_2$ for 0, 1, 6, 24 and 72 h, are shown in Fig. 3.

It has been reported that the mature bean (*Phaseolus vulgaris*) tissue showed swelling of the thylakoids within the chloroplasts without any extrachloroplast damage after exposure towards 1 and 2 μL L^{-1} of NO$_2$ for 1 and 2 h, and the swelling of the thylakoid could be inverted by removal of the air pollutant or by a change in the rate of gas flow within the tissue.[31] Li *et al.* studied the NO$_2$ assimilation capacity of 70 woody plants. They demonstrated that deciduous broad-leaved trees possessed the maximum growth rate under high-concentration NO$_2$ stress, with *Robinia pseudoacacia*, *Sophora japonica*, *Pterocarya stenoptera*, and *Cerasus serrulate* showing the highest recovery among them.[27] The common symptoms experienced by several plants towards NO$_x$ exposure, such as chlorosis of young needles and tip burn of older needles, were frequently detected in coniferous species.[33] Herringbone necrosis has been observed in the older leaves of beech, hazel, and apple trees. Various plant species demonstrate a water-soaked appearance on their leaves, which is followed by necrosis on exposure towards acute NO$_x$. Moreover, leaf glazing has been detected in the plants of the annual pea, cabbage, and spinach.[32]

Air pollutants such as NO$_2$ can indirectly influence vegetation by chemical reactions in the atmosphere, and directly affect vegetation, soil, or water after deposition. The effect of pollutants on plants is considered by their adsorption and rate of uptake (flux) and the plant's reaction.[4] High levels of nitrogen dioxide are detrimental for vegetation as it results in damage to foliage, a decrease in growth, and a reduction in crop yields.

In view of the above, it is necessary to determine the ecological and environment-friendly monitoring techniques to reduce atmospheric NO$_2$ concentrations. Therefore, researchers are trying to fabricate low cost, easy to process, fast response/recovery, selective, highly sensitive, and low operation temperature NO$_2$ sensors.

3. Different techniques for monitoring NO$_2$

The chemical sensor consists of a transducer and an active layer that converts chemical information into another form of an electronic signal, such as a frequency change, a voltage change, or a current change. Various gas sensor technologies, such as catalytic gas sensors, electrochemical gas sensors, semiconductor gas sensors, acoustic gas sensors, and optical
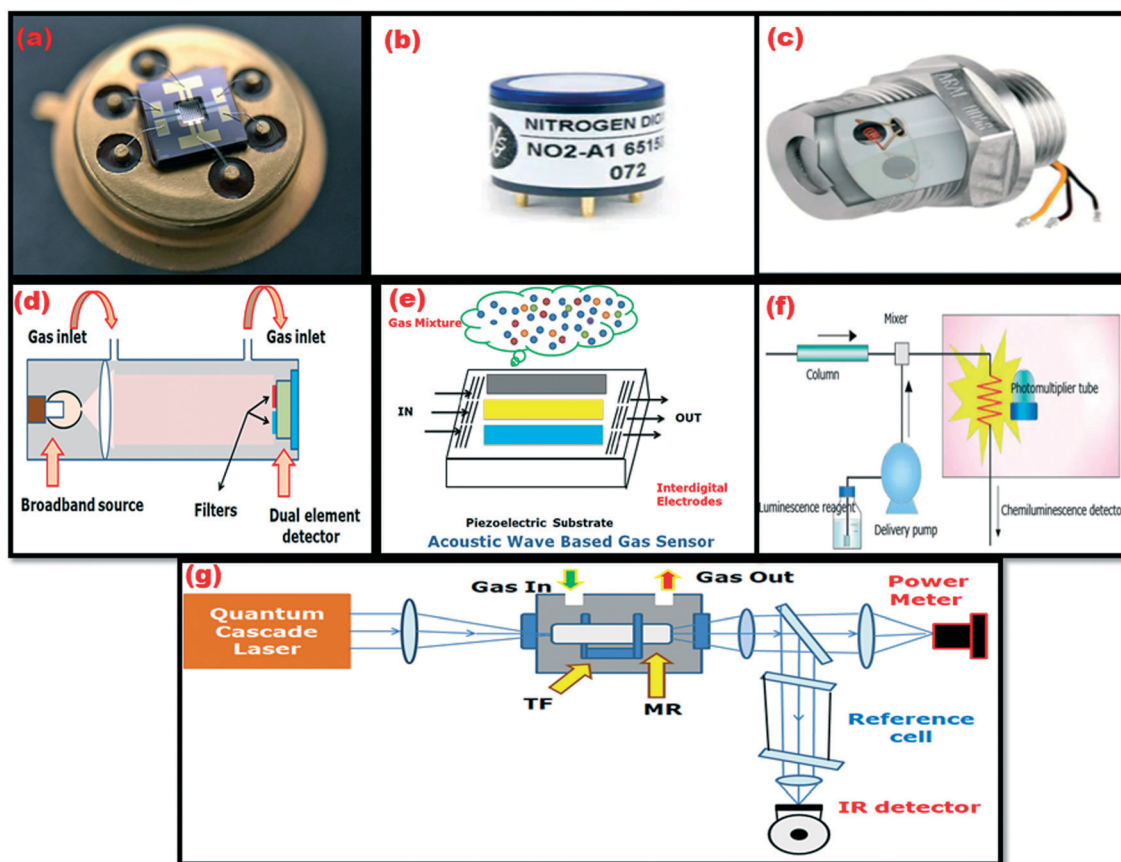

Fig. 4 Different NO$_2$ gas sensors: (a) MOS sensor,[44] (b) electrochemical sensor,[45] (c) catalytic sensor,[46] (d) optical sensor, (e) acoustic wave sensor, (f) chemiluminescence and (g) photoacoustic spectroscopy.

gas sensors, have been used to detect NO$_2$ gas. The various NO$_2$ gas sensors, such as the MOS sensor, electrochemical sensor, catalytic sensor, optical sensor, acoustic wave sensor, chemiluminescence, and photoacoustic spectroscopy, are shown in Fig. 4. Table 1 displays the advantages/disadvantages associated with each technique.

The sensing mechanism of each sensor depends on various properties, such as the operating temperature, selectivity, response time, detection limit, sensitivity, and recovery time, which are also well defined in a later section of this article.

3.1 Catalytic sensors

For almost a century, catalytic sensors have been used to detect combustible gases. Jonson discovered the first catalytic combustion type sensor in 1923.[33,34] Combustible gas mixtures do not burn until they attain a certain ignition temperature. However, in the presence of a particular chemical process, the gas will start to ignite even at lower temperatures.[35] This process is called catalytic combustion. A gas sensor made based on the catalytic principle is called a catalytic gas sensor. The catalytic gas sensor is classified into two types – thermoelectric type and Pallister type.[35]

3.2 Electrochemical gas sensors

Electrochemical gas sensors allow gases to diffuse through a porous membrane to an electrode, where they are reduced or oxidized. These sensors work by reacting with a target gas and generating an electrical signal that is proportional to the gas concentration. These gas sensors are composed of a working electrode and a counter electrode, which are detached by a thin layer of electrolyte. Potentiometric, amperometric and conductometric are the categories of the electrochemical gas sensors. In these types of sensors, the

resultant quantities, such as the potential, current, and frequent series of conductivities of the electrode, are measured.[36] Laref *et al.* evaluated the performance of a four-electrode electrochemical sensor for in-field nitrogen dioxide monitoring, and also proposed an empirical unsupervised recalibration method. This study revealed the effectiveness of the proposed drift correction approach.[37]

3.3 Optical gas sensors

Optical gas sensors utilize optical absorption/emission scattering of gas molecules at determined optical wavelengths. Optical gas sensors comprise a photodetector component, a light-emitting element, a gas sensing element, and a filter for getting phosphorescence or fluorescence. Thin films of palladium or chemochromic oxides are generally used in most optical sensors. These thin films of oxides are coated along the length of an optical fiber and it is known as optodes. An infrared gas sensor is an example of this category.[38] Paliwal *et al.* developed a low-cost tabletop surface plasmon resonance system. They incorporated the RF magnetron sputtered WO$_3$ thin film with a gold-coated prism to excite the surface plasmon modes in the Kretschmann configuration (WO$_3$/Au/prim). The WO$_3$ thin film deposited at a sputtering pressure of 50 mT exhibited a very sharp SPR curve with a low value of reflectance (0.21) at the resonance angle of 46.6°. NO$_2$ gas was detected at room temperature by the optimized system (WO$_3$ (50 mT)/Au/prim). The WO$_3$/Au/prism SPR system was found to be suitable for the selective detection of low concentrations of NO$_2$ gas (0.5 ppm) with high sensitivity.[39]

3.4 Acoustic wave sensors

The detection principle of acoustic wave sensors is based on a mechanical or acoustic wave. When the acoustic wave propagates through the material, a particular change is

Table 1 Different NO$_2$ detection techniques with their advantages and disadvantages

Name of the sensing technique	Measured quantities	Working principle	Advantages	Disadvantages
MOSs-based sensors	Conductivity	Conductometric	Low cost and long lifetime, wide range of target gases	Sensitivity to environmental components, high energy consumption, non-selective
Catalytic sensor	Temperature, resistance	Catalytic/gas oxidation	Simple and low-cost measures flammability of gases	Need of air or oxygen to work
Optical sensor	Polarization, light intensity, wavelength, *etc.*	Fluorescence, optical, *etc.*	Easy to operate in the absence of oxygen, unaffected from electromagnetic interference	High cost and miniaturization
Electrochemical sensor	Charge, current, resistance, voltage, inductance, *etc.*	Potentiometric, amperometric, resistive, *etc.*	Ability to measure toxic gases in low concentration	Easy contamination
Mass resistive sensor/acoustic wave sensor	Change in the characteristics such as velocity and amplitude	Acoustic	Long lifetime and no secondary pollution	Sensitive to environmental factors
Photoacoustic spectroscopy	Absorbed electromagnetic energy	Photoacoustic	High sensitivity	Miniaturization, stability
Chemiluminescence (fluorescence)	Dark current/photocurrent	Emission of radiation	Quick response high sensitivity	Non-linear behavior

noticed in the characteristics of the wave (amplitude/velocity). The variation in velocity can be monitored by measuring the phase or frequency characteristics of the sensor. These sensors consist of a receptor and a transducer, which are sensitive to an analyte and convert the response into an electrical signal, respectively.[36,40] Li *et al.* used a cation-exchange method to synthesize PbS CQDs to enhance the performance of the SAW sensor. The Pb(NO3)$_2$-treated sensor showed potential for monitoring traces of NO_2 in the concentration range of 0.5–30 ppm with good sensitivity and selectivity at room temperature.[41]

3.5 Chemiluminescence

Emission of UV, IR, or Vis radiation by a chemical reaction or reactions defines a luminescent phenomenon that is widely known as chemiluminescence (CL). As an analytical technique, CL detection is widely known for its quick response, high sensitivity, and absence of undesirable luminescence in the background. This emission can be seen in the solid, liquid, and gas phases.[42] In this manner, it can facilitate and widen its area of analytical applications. Among these gas phases, liquid-phase CL exhibits significant potential for analytical applications, while gas-phase CL plays a vital role in monitoring and measuring several gaseous and volatile elements in the environment.[43]

3.6 Photoacoustic spectroscopy

Gas-phase spectroscopy is currently extremely famous in a wide scope of fields, for example, biology, atmospheric, chemistry, and medical sciences. This spectroscopy depends on the photoacoustic effect, which was first described by Alexander Graham Bell.[47] The spectroscopic gas sensors have proved to be worthwhile tools. For specific gas compounds, some applications require a sensor that can detect a wide range of gases, while others need high sensitivity. There is also a desirable selectivity, time resolution, and robustness. In this technique, there is no need for maintenance and sample preparation.[48] Peltola *et al.* demonstrated a simple and highly sensitive cantilever enhanced photo-acoustic sensor for the detection of nitrogen dioxide at 532 nm. It was observed that the sensitivity of the setup was enhanced by approximately a factor of eight for an averaging time of 120 s, and a CEPAS signal with a high laser power improved the NO_2 detection limit to as low as a few parts-per-trillion.[49]

4. Metal oxide semiconductor (MOS) gas sensors

Metal oxides are recognized as suitable materials for gas sensor and biosensor applications. The surface of these materials possesses effective interaction with gas molecules. Using various tailoring techniques, the surface properties of metal oxide permit enhanced sensing properties. Reduction in the grain size at the nanoscale leads to a large active surface area, and induces novel effects like bandgap widening
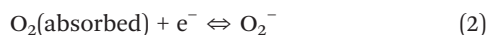
and room temperature photoluminescence due to quantum confinement. These innovative physical properties in the metal oxide nanostructures pave the way for the advancement in sensor technology with advanced parameters. Metal oxide nanomaterials with desired properties, such as composition, stoichiometry, phase control, and geometry, can be achieved by different synthesis methods. In order to achieve these properties, various synthesis methods, such as chemical vapor deposition, electro-deposition co-precipitation, sol–gel, thermal decomposition, microemulsion, solvothermal, and microwave-assisted methods, have been widely explored by researchers.[50] Various metal oxides, such as Fe_2O_3, ZnO, CuO, NiO, WO_3, TiO_2, MgO, and SiO_2, have been synthesized using these methods. Many efforts have been done by researchers in the last few years to improve the sensitivity of gas sensors. Metal oxides with different nanostructures, such as nanowires, nanofibers, nanotubes, nanosheets, and nanospheres, display excellent gas sensing properties as they possessed a large surface area and relatively mass reactive sites.[51] In the vapor deposition process, metal oxides grow from atoms or molecules *via* the vapor–solid or vapor–liquid–solid process. Diverse morphologies, such as nanowires, nanorods, nanoribbons/belts, 2D nanosheets, and 3D hierarchically-ordered microstructures, have been achieved by controlling the parameters.[52] The synthesis of metal oxide nanostructures by anodic oxidation or electrodepositions results in nanofibers, nanowires, nanorods, nanotubes, and 3D nanoflowers. Meanwhile, in the surfactant-assisted synthesis process, surfactants in the form of micelles and microemulsions are employed as templates, thus providing nanoparticles, 1D nanowires, nanorods, nanoribbons, nanotubes, and 3D nanospheres structures.[53] Metal oxide nanotubes and nanowires are mostly prepared through the hydrothermal method, anodizing processes, and sol–gel method. For example, SnO_2 nanowires prepared through glycolate precursors under mild conditions displayed good sensitivity towards certain gases, such as C_2H_5OH, CO, and H_2. Meanwhile, SnO_2 nanotubes using the multi-walled carbon nanotube (MWCNT) as a template prepared by the wet chemical method were more porous and showed excellent response towards ethanol and acetone.[54] In recent years, metal oxides have been widely studied as sensing materials for NO_2 gas sensing.[55] The metal oxide semiconductor gas sensors are composed of a sensitive metal oxide surface layer. The gas concentration of a target gas is measured by these metal oxides *via* measuring the electrical resistance. These sensors are based on the reversible gas adsorption process at the surface of the metal oxide.[38] Xin *et al.* synthesized a novel composite of PbS quantum-dots-modified MoS_2 by the combination of the hydrothermal method with the chemical precipitation method, and then fabricated into the gas sensor. It was found that the response of MoS_2/PbS is higher than that of the pure MoS_2 gas sensor, and the MoS_2/PbS gas sensor showed better selectivity compared with the pure MoS_2 gas sensor at room

temperature. The response of the MoS_2/PbS gas sensor was about 50 times higher than that of the MoS_2 gas sensor at 100 ppm NO_2 concentration, and the recovery rate was also improved.[56]

The gas sensing mechanism of MOS-based sensors

At first, when the MOS surface layer is heated in air, oxygen is adsorbed on the surface of the metal oxide. In this process, the adsorption of oxygen forms an ionic species, such as O_2^-, O^- and O^{2-}, and these species obtained electrons from the conduction band. The kinematics of this adsorption process can be explained *via* these eqn (1)–(4)[57,58]

$$O_2(gas) \Leftrightarrow O_2(absorbed) \tag{1}$$

$$O_2(absorbed) + e^- \Leftrightarrow O_2^- \tag{2}$$

$$O_2^- + e^- \Leftrightarrow 2O^- \tag{3}$$

$$O^- + e^- \Leftrightarrow O^{2-} \tag{4}$$

These oxygen species are stable at different temperatures; for example, O_2^- shows stability at 100 °C, and O^- shows stability between 100 and 300 °C, while O^{2-} is stable above 300 °C.[59] When an electron transfers from the conduction band to chemisorbed oxygen, then there is a reduction in the electronic concentration. It is observed that the resistance increases for the n-type semiconducting metal oxide, while it decreases for the p-type metal oxide. Fig. 5(a) describes the mechanism of the decrease in resistance as the conduction increases in the case of the n-type MOS sensor. Sensing properties depend on the operating temperature, and this

dependence could result in the change in adsorption and desorption rates of oxygen ions at the metal oxide surface.[60] Generally, environmentally unsafe gases can be classified into two categories depending on their oxidizing and reducing effects. H_2S, CO, NH_3, CH_4, and SO_2 gases fall in the group of reducing gases, while NO_2, NO, N_2O, and CO_2 gases fall into in the oxidizing group. When metal oxide surfaces are exposed to oxidizing gases, then these target gases react with the adsorbed O^- ions and adsorb directly on the surface of the metal oxide. NO_2 is a strongly oxidizing gas. When the molecules of this gas interact with the metal oxide surface through adsorbed oxygen ions, the potential barrier consequently increases at the grain boundaries.[61,62] As a result, the thickness and resistance of the depletion layer increase, as shown in Fig. 5(b).

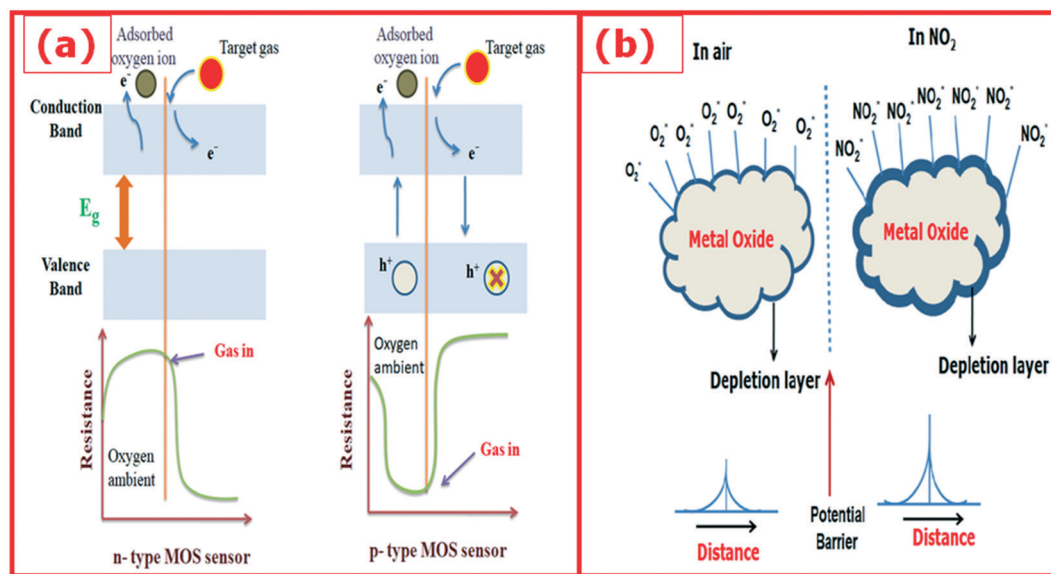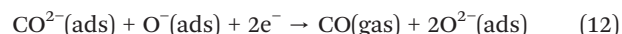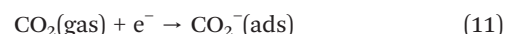The oxidizing reactions for different oxidizing gases are given as ((5)–(12)):[63–69]

$$NO_2(gas) + e^- \rightarrow NO_2^-(ads) \tag{5}$$

$$NO^{2-}(ads) + O^-(ads) + 2e^- \rightarrow NO(gas) + 2O^{2-}(ads) \tag{6}$$

$$NO(gas) + e^- \rightarrow NO^-(ads) \tag{7}$$

$$2NO^-(ads) \rightarrow N_2(gas) + 2O^-(ads) \tag{8}$$

$$N_2O(gas) + e^- \rightarrow N_2O^-(ads) \tag{9}$$

$$N_2O^-(ads) \rightarrow N_2(gas) + O^-(ads) \tag{10}$$

$$CO_2(gas) + e^- \rightarrow CO_2^-(ads) \tag{11}$$

$$CO^{2-}(ads) + O^-(ads) + 2e^- \rightarrow CO(gas) + 2O^{2-}(ads) \tag{12}$$
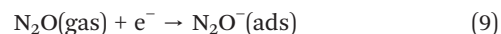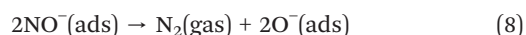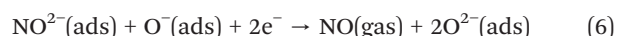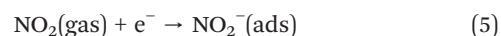

Fig. 5 (a) Schematic diagram: sensing mechanism of n-type and p-type MOSs. (b) The interaction of oxygen and NO_2 with n-type semiconducting metal oxides. Charge distribution following the adsorption of oxygen (left) and NO_2 (right) on the surface of the metal oxide. The resulting potential distribution across the grain boundaries is also shown in the figure.
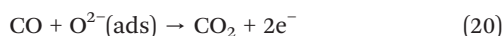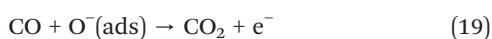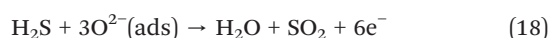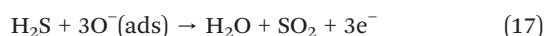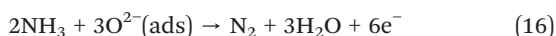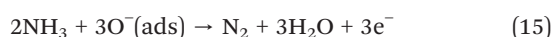
For the oxidizing gas, the gas sensing response for n-type (S_{ox}^n) and p-type (S_{ox}^p) semiconducting oxide is generally explained by these eqn (13) and (14):

$$S_{ox}^n = R_{og}/R_a [\text{n-type}] \quad (13)$$

$$S_{ox}^p = R_a/R_{og} [\text{p-type}] \quad (14)$$

where R_{og} and R_a are the electrical resistances of the sensors in the presence of the target oxidizing gas and pure air.

On the other hand, when metal oxide surfaces are exposed to reducing gases, the gas reacts with the chemisorbed oxygen by releasing an electron and goes back to the conduction band. The reducing reactions between the chemisorbed oxygen species and reducing gases are generally given as eqn (15)–(20).[70–82]

$$2NH_3 + 3O^-(\text{ads}) \rightarrow N_2 + 3H_2O + 3e^- \quad (15)$$

$$2NH_3 + 3O^{2-}(\text{ads}) \rightarrow N_2 + 3H_2O + 6e^- \quad (16)$$

$$H_2S + 3O^-(\text{ads}) \rightarrow H_2O + SO_2 + 3e^- \quad (17)$$

$$H_2S + 3O^{2-}(\text{ads}) \rightarrow H_2O + SO_2 + 6e^- \quad (18)$$

$$CO + O^-(\text{ads}) \rightarrow CO_2 + e^- \quad (19)$$

$$CO + O^{2-}(\text{ads}) \rightarrow CO_2 + 2e^- \quad (20)$$

In the case of reducing gases, the gas sensing response for n and p-type semiconducting oxide is given by eqn (21) and (22):

$$S_{rd}^n = R_a/R_{rg} [\text{n-type}] \quad (21)$$

$$S_{rd}^p = R_{rg}/R_a [\text{p-type}] \quad (22)$$

where R_{rg} and R_a are the electrical resistances of the sensor in the presence of the target oxidizing gas and pure air, respectively.

The gas sensing response of the MOS sensors relies on the ratio between the thickness of the depletion layer and the bulk semiconductor. Additionally, various other factors determine the gas-sensing mechanism of the specific nanostructured metal oxides semiconductors (NMOS). In these factors, the surface-to-volume ratio is an important factor, *i.e.*, if the size of the metal oxide nanoparticles decreases, the number of adsorbed gas molecules increases, and then it results in a higher gas response.[83] The gas response strongly depends on the diameter, *i.e.*, shape and size of the nanorods/nanowires of the metal oxides. If the metal oxide nanorods/nanowires have a small diameter, it directly suggests that more atoms are available for surface reactions.[84,85]

For practical use, the gas sensors must meet various requirements based on the interesting field of application. These requirements are described by some fundamental properties of a gas sensor. The most commonly used gas sensing parameters with their definitions are summarized below:

Sensitivity

It is concerned with the changes in electrical resistance of the sensing layer due to the adsorbed or chemisorbed species of the oxidizing or reducing gas in its contact.[86]

Selectivity

The selectivity of any gas sensor is determined by the sensor's ability to differentiate the desired gas from the mixture of gases at the same concentration level.

Response

When the sensor is exposed to an analyte gas, then the resistance of the sensor is changed. This change in resistance as a function of analyte gas concentration is defined as a response.

$$\text{Response (\%)} = \left[\frac{R_g - R_a}{R_a}\right] \times 100$$

where R_a and R_g show the respective sensor resistance in air and analyte gas, respectively.[87]

Response time and recovery time

The response time is the time required for achieving 90% of the final sensor signal,[88] while the recovery time is defined as the time required by the sensor to reach 10% of the baseline value.

Limit of detection

LOD is defined as the capability of a gas sensor to measure the least possible concentration of the analyte gas with reliability under the given conditions.

Working temperature

The temperature at which the gas sensor shows the highest response for a certain amount of the analyte gas is known as the working temperature of a gas sensor.[52]

Repeatability

The repeatability of a sensor is defined as when it shows the same characteristics, such as response, sensitivity, and selectivity over the repeated tests.

Stability

Stability stands for the ability of a sensor to retain its properties when continuously operated over a longer time.

Table 2 Summary of various NMOS-based NO$_2$ gas sensors with their sensing parameters

Material	Structure	Synthesis method	Target gas	C (ppm)	Operating temp. (°C)	Response	t_{res}/t_{rec}	LOD	Ref.
ZnO	Nanowalls	Solution	NO$_2$	50	RT	~6.2	23/11 s	~5 ppm	89
NiO/WO$_3$	Plates	Annealing	NO$_2$	30	RT	4.8	2.5/1.1 s	5 ppm	124
WO$_3$/S/rGO	Nanorods	Hydrothermal	NO$_2$	20	RT	149.5	6/56 s	0.25 ppm	125
NiO/rGO	Nanosheets	Hydrothermal	NO$_2$	0.25	RT	0.04	576/121 s	~0.25 ppm	126
ZnO	Nanowires	Drop-cast	NO$_2$	20	RT	32	72/69 s	~5 ppm	90
NiO/SnO$_2$	Nanosheets	Annealing	NO$_2$	60	RT	~7.5	—	~5 ppm	102
ZnO/rGO	Nanowalls	Solution	NO$_2$	50	RT	9.61	25/15 s	~5 ppm	117
CuO/rGO	Nanosheets	Chemical solution	NO$_2$	1	RT	14	66/34 s	60 ppb	114
ZnO			NO$_x$	1	RT		240/— s	10 ppb	91
SnO$_2$/S/rGO	Nanoparticles	Hydrothermal	NO$_2$	5	RT	20.31	40/357 s	1 ppm	127
ZnO	Nanorods	Wet chemical route	NO$_2$	1	RT	100	~5/~20 min	~1 ppm	128
α-Fe$_2$O$_3$/rGO	Nanospheres	Hydrothermal	NO$_2$	90	RT	150.63	—/1648 s	0.18 ppm	129
ZnO	Nanowires	CVD	NO	10	RT	46	—	1.5 ppm	130
NiO/CuO	Flower-like	Hydrothermal	NO$_2$	100	RT	77.16	2 s/—	1 ppm	131
SnO$_2$	Nanotubes	Electrospinning	NO$_x$	9.7	RT	89.2	6/218 s	9.7 ppb	97
In$_2$O$_3$/rGO	Layers	Reflux	NO$_x$	97	RT	1.45	25/— s	970 ppb	132
SnO$_2$	Nanocrystals	Chemical precipitation	NO$_2$	11	RT	33	100/250 s	~3 ppm	133
ZnO			NO$_x$	1	200		60/— s	0.1 ppm	134
In$_2$O$_3$/SnO$_2$	Nanorods	Electrospinning	NO$_x$	100	RT	8.98	4.67/— s	0.1 ppm	118
SnO$_2$	Thin films	Pulsed laser deposition	NO$_2$	4	RT	7730	3/176 s	~4 ppm	92
CeO$_2$/graphene	Nanosheets	Solvothermal	NO$_x$	300	RT	12.76	1.3/— s	5 ppm	135
In$_2$O$_3$	Octahedra	Sol–gel	NO$_2$	200	RT	~70	~500/~500 s	0.1 ppm	136
SnO$_2$/rGO	Nanoparticles	Hydrothermal	NO$_2$	1	RT	3.8	14/190 s	50 ppb	121
SnO$_2$	Nanowires	—	NO$_2$	10	RT, UV assisted	~85	10/15 min	~0.1 ppm	93
In$_2$O$_3$	Mesoporousnanocrystals	Hydrothermal	NO$_x$	97	RT	158.7	96/— s	970 ppb	19
TiO$_2$	Thin films	Rf-Sputter	NO$_2$	250	RT, UV assisted	~1.8	100/210 s	100 ppm	137
TiO$_2$	Nanodots	Nano-oxidation	NO	10	RT	31	91/184 s	~5 ppm	138
In$_2$O$_3$/TiO$_2$	Nanofibers	Electrospinning	NO$_x$	97	RT	41.1	3/— s	97 ppb	119
TiO$_2$	Nanoparticles	Hydrothermal	NO$_2$	40	RT	1093	48/52 s	0.02 ppm	94
In$_2$O$_3$	Nanoparticles	Ultrasonic spray pyrolysis	NO$_x$	100	250		600/— s	0.1 ppm	20
Cu$_x$O/graphene	Nanoflowers	Reflux	NO$_x$	97	RT	95.1	9.6/— s	97 ppb	139
ZnO/SnO$_2$	Nanorods	Wet chemical	NO$_2$	0.5	RT, UV assisted	1266	7/8 min	~200 ppb	120
MoO$_3$	Thin films	Magnetron sputtering	NO	200	RT	92	30/1500 s	5 ppm	140
Al$_2$O$_3$/TiO$_2$	Nanotubes	Induction	NO$_x$	97	RT	88.04	~8/~8 s	0.97 ppm	141
WO$_3$	Nanoplates	Chemical	NO$_x$		300		80/— s	0.5 ppm	95
ZnO$_{1-x}$	Sheet-like	Suspension flame spraying	NO$_2$	1	RT	~2.568	60/230 min	0.25 ppm	142
MWCNTs/WO$_3$	Nanoparticles	Hydrothermal	NO$_2$	5	RT	14	10/27 min	0.1 ppm	143
PdO/Co$_3$O$_4$	Nanocubes	Chemical precipitation	NO$_2$	20	RT	27.33	—	1 ppm	144
CuO	Microspheres	Reflux method	NO$_x$	97	RT	64.93	5.33/— s	0.97 ppm	98
WO$_3$	Hollow microspheres	Hydrothermal	NO$_x$	2.5	300		—	0.5 ppm	145
K$_2$O/In$_2$O$_3$	Nanowires	Template	NO$_x$	97	RT	151.78	12/— s	48.5 ppb	146
α-Fe$_2$O$_3$/rGO	Nanoparticles	Hydrothermal	NO$_2$	5	RT	3.86	76/946 s	0.1 ppm	147
Cu$_2$O/rGO	Nanoparticles	Chemical solution	NO$_2$	1	RT	5.2	29.2/76.8 s	100 ppb	148
ZnO	Microwires	Surface etching	NO$_2$	20	RT, UV assisted	411	221/118 s	~10 ppm	149
ZnO/graphene	Spheres	Solvothermal	NO$_2$	50	RT	8	132/164 s	~1 ppm	150
Co$_3$O$_4$/rGO	Thin sheets	Hydrothermal	NO$_2$	800	RT	~8	1.5/1 min	60 ppm	151
ZnO	Nanoparticles	Hydrothermal	NO$_2$	20	RT, UV assisted	85	26/16 s	~1 ppm	152
In$_2$O$_3$/rGO	Nanosheets	Hydrothermal	NO$_2$	30	RT	8.25	4/24 min	~5 ppm	153
SnO$_2$/graphene	Nanoparticles	Sol–gel	NO$_2$	20	RT	~9.5	1/5 min	5 ppm	154
CuO	Virus-like	Chemical solution	NO$_2$	4	RT	28.1	22/42 s	1 ppm	99
SnO$_2$	Nanoparticles		NO$_x$		300			0.5 ppm	155

Table 2 (continued)

Material	Structure	Synthesis method	Target gas	C (ppm)	Operating temp. (°C)	Response	t_{res}/t_{rec}	LOD	Ref.
Pd/ZnO	Nanoparticles	Sol–gel	NO$_2$	50	RT	45.2	67/250 s	10 ppm	106
WO$_3$/MWCNT/rGO	Nanoparticles	Hydrothermal	NO$_2$	5	RT	17	7/15 min	1 ppm	156
In$_2$O$_3$	Nanostructures	Arc-discharge	NO	50	RT, UV assisted	41.7	~10/— min	~2 ppm	157
Au/SnO$_2$	Nanoparticles	Sputtering	NO$_2$	50	RT	90	70/— s	600 ppb	113
CuO	Nanoplatelets	Sonochemical method	NO$_2$	40	RT	53 737	—	—	100
WO$_3$	Nanoparticles	Chemical	NO$_x$		350		180/— s	1 ppm	158
Ag/SnO$_2$/rGO	Nanoparticles	Hydrothermal	NO$_2$	5	RT	2.17	49/339 s	1 ppm	110
NiO	Nanosheets	Microwave synthesis	NO$_2$	10	RT	0.56	—	—	101
Au/VO$_2$	Nanowires	CVD/ion sputtering	NO$_2$	5	RT	3.22	~50/~600 s	~0.5 ppm	109
Pd/Ga$_2$O$_3$	Nanowires	Thermal evaporation	NO$_2$	100	RT	41.44	200/70 s	~10 ppm	107
SnO$_2$	Nanofibers	Chemical	NO$_2$	5	200		85/110 s	1 ppm	159
CeO$_2$/rGO	Bilayer	Spray	NO$_2$	10	RT	20.5	92/— s	~1 ppm	160
SnO$_2$/rGO	Nanoparticles	Hydrothermal	NO$_2$	1000	RT	22.87	100/— s	1 ppm	122
Fe$_3$O$_4$/graphene	Nanoparticles	Hydrothermal	NO$_2$	400	RT	24.2	275/738 s	~30 ppm	161
ZnO/rGO	Nanorods	Oriented growth	NO$_2$	1	RT	119	75/132 s	50 ppb	162
NiO	Nanosheets	Hydrothermal	NO$_2$	60	RT	3.05	~200/~300 s	~5 ppm	102
Al/NiO	Nanosheets	Solvent-thermal	NO$_2$	10	RT	2.77	50/200 s	250 ppb	101
NiO	Nanosheets	Hydrothermal	NO$_2$	60	RT	1.8	~250/~250 s	~7 ppm	103
Cu/Cu$_2$O	Hollow spheres	Hydrothermal	NO$_2$	10	RT	6.27	34/— s	—	111
Co$_3$O$_4$	Nanoparticles	Thermal treatment	NO$_x$	100	RT	52.1	—	100 ppb	104
Sb/WO$_3$	Nanoparticles	Chemical solution	NO$_2$	10	RT	51	~150/~200 s	~1 ppm	96
WO$_3$/MWCNTs	Nanoparticles	Metal organic decomposition	NO$_2$	0.1	RT	0.25	10.5/20 min	100 ppb	163
Cellulose/Fe$_2$O$_3$	Nanoparticles	Hydrothermal	NO$_2$	200	RT	~1100	50/30 s	1 ppm	164
WO$_3$-δ	Films	Granule spray	NO$_2$	10	RT	18 500	17/25 s	1.88 ppm	165
CNT	Thin films		NO$_2$	100	165		~30 min	10 ppm	112
Co$_3$O$_4$	Flower-like	Hydrothermal	NO$_2$	60	RT		~25/70 s	—	105
SnO$_2$-CuO/rGO	Composite	Hydrothermal	NO$_2$	50	RT	~250%		150 ppb	166
α-Fe$_2$O$_3$	Thin film	Hydrothermal	NO$_2$	100	RT	~86%	~31/32 s	—	167
V$_2$O$_5$	Microbelts	Mold-casting	NO$_2$	100	RT		~35/47 s	—	168
N-GQDs/ZnO composite	Nanosheet to spherical	Hydrothermal	NO$_2$	05	100 °C	~22%	—	0.1 ppm	169
CuO/rGO	Nanoflakes	Hydrothermal	NO$_2$	05	RT	~400.8%	6.8/55.1 s	50 ppb	115
SnO$_2$/RGO	Spherical	Hydrothermal	NO$_2$	100	250 °C	~88.9	12/34	—	116
SnO$_2$	Nanowires	Lithography and thermal evaporation	NO$_2$	05	RT	~50	7 min/100 s	—	170
CuO/ZnO	Nanowires	Thermal oxidation and sol–gel	NO$_2$	100	250 °C	~4.1	25/150 s	—	171
Cd-Doped Co$_3$O$_4$	Nanosheet	Microwave-assisted solvothermal	NO$_2$	10	RT	~3.38	—	154 ppb	172

5. Nanostructured metal oxides semiconductors (NMOS)-based NO$_2$ gas sensors

Various n-type MOSs-based gas sensors, such as ZnO,[89–91] SnO$_2$,[92,93] In$_2$O$_3$,[77] TiO$_2$,[94] and WO$_3$,[95] have been studied for their excellent gas-sensing performance (response/recovery time (t_{res}/t_{rec}), selectivity, operating temperature (°C), and LOD) for NO$_2$, as listed in Table 2. One of the most outstanding features of the MOS-based NO$_2$ gas sensors is their fast response due to the strong oxidation of the NO$_2$ molecules.[96] The ZnO cross-linked nanowalls with a pore size of (200 nm to 500 nm) exhibited fast response/recovery times of 23/11 s and a high response value (6.4) towards 50 ppm NO$_2$ at RT with good repeatability.[89] The ZnO hierarchical nanostructure-based gas sensor prepared by drop-cast method showed a significant 28-fold improvement over the traditional widely adopted nanowire-based gas sensor with a fast response/recovery time of 72/69 s at RT for 20 ppm NO$_2$.[90] The sensor based on the SnO$_2$ material with a tube-like structure (5–10 nm) exhibited a very fast response time of 6 s and a low LOD of 9.7 ppb at RT. The sensing action was due to the nanocrystalline SnO$_2$ grains

and the high density of defects (twin boundaries & dislocations).[97] The sensor using mesoporous In_2O_3 was reported with its high response value of 158.7 towards 97 ppm NO_2, with a fast response time of 96 s and a low LOD of 970 ppb at RT.[19] The sensor made of TiO_2 nanoparticles (6.5 nm) prepared by hydrothermal method exhibited an ultra-high response of the value of 1093 to 40 ppm NO_2, fast response/recovery times (48/52 s), and a low LOD of 0.02 ppm at RT, but the selectivity among NH_3, H_2 and CH_4 was very poor.[94] The large surface area and pore volume of the TiO_2 nanoparticles provide a high concentration of oxygen vacancies and interstitial defect states on the surface. Thus, efficient adsorption and desorption of NO_2 gas molecules are feasible methods that can result in high sensitivity of the sensor.

P-Type nanostructures, such as CuO,[98–100] NiO,[101–103] and Co_3O_4,[104] have also been reported as good NO_2 sensing materials. Hierarchical CuO microspheres prepared by using the facile reflux method exhibited high sensitivity of 64.9 and response time of 5.33 s to 97 ppm at RT. Good selectivity, stability, and low LOD of 0.97 ppm NO_x gas are the other advantages of these sensors. This was attributed to the hierarchical structure of the CuO microspheres that allows for effective and rapid gas diffusion towards the sensing surfaces.[98] The sensor based on CuO virus-like microspheres synthesized by the chemical solution method exhibited a high response of 28.4 and response/recovery

times of 22/42 s towards 4 ppm NO_2 at RT.[99] CuO nanoplatelets-based NO_2 gas sensors prepared by sonochemical method revealed an ultra-high response to 40 ppm NO_2 operated at RT. This sensor exhibited good sensitivity, selectivity, and low power consumption due to the small crystallite size, higher surface area, and point defects.[100] The NO_2 gas sensors were also prepared using self-assembled polycrystalline hexagonal mesoporous NiO nanosheets,[102,103] and the sensors showed much better responses to NO_2 operated at room temperature. The micro flowers-like Co_3O_4 structures have also been synthesized using a low-cost single-step hydrothermal method.[104] The hierarchical 3D flower-like Co_3O_4-based sensor has a fast response/recovery time of the order ~25/70 s and good selectivity towards 60 ppm NO_2 at RT. In a recent investigation, Kumar et al.[105] synthesized Co_3O_4 flower-like structures using the hydrothermal method. It was also noticed that the 3D flower-like Co_3O_4 (Fig. 7d) sensor at RT attained the maximum response to 60 ppm of NO_2 gas at ~22%, and these hierarchical 3D micro flowers might become the reason for the improved sensor response. In this way, the Co_3O_4 sensor could be a promising candidate for NO_2 detection at RT. The resistance response during cyclic exposure at different and fixed concentrations, sensor response versus different chemical inputs and stability of the sensor at RT are shown in Fig. 7a, b, c, e and f, respectively.[105]
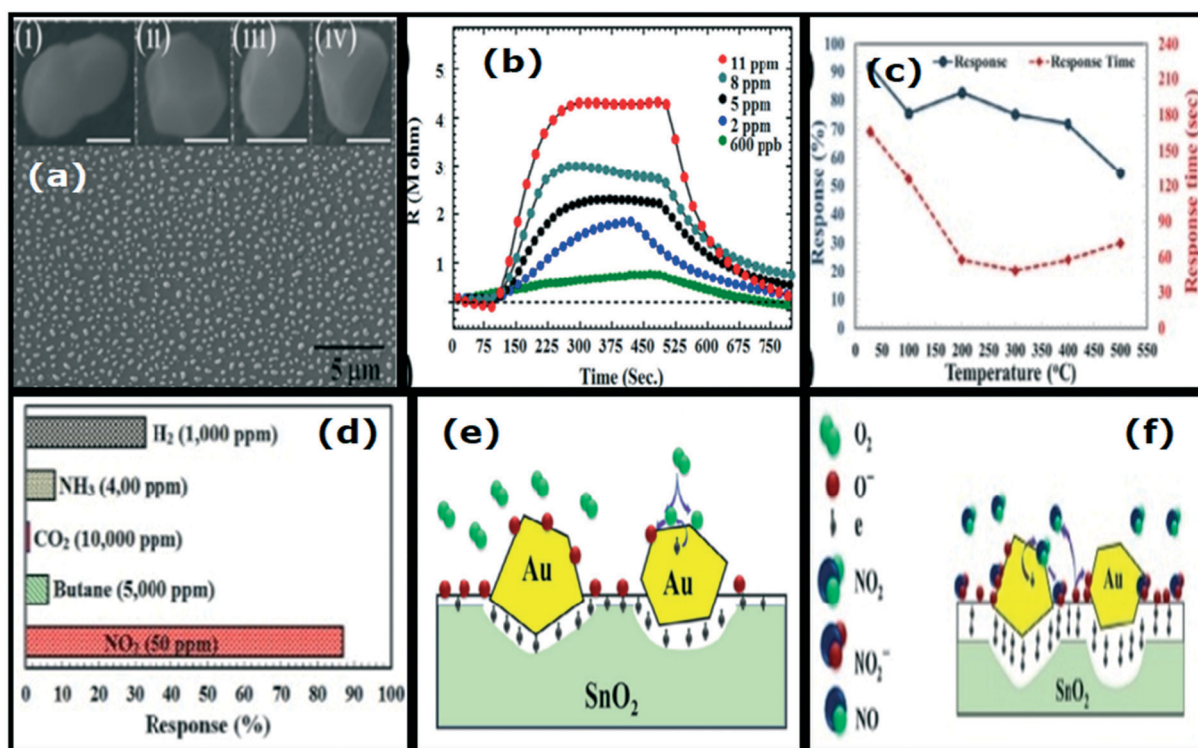

Fig. 6 (a) SEM image of the Au/SnO_2 thin film, (b) response-recovery curves of the Au/SnO_2 sensor in various concentrations of NO_2, (c) response and response time at different operating temperatures, (d) selectivity of the fabricated sensor for various target gases, and (e and f) the schematics of the sensing mechanism.[113]
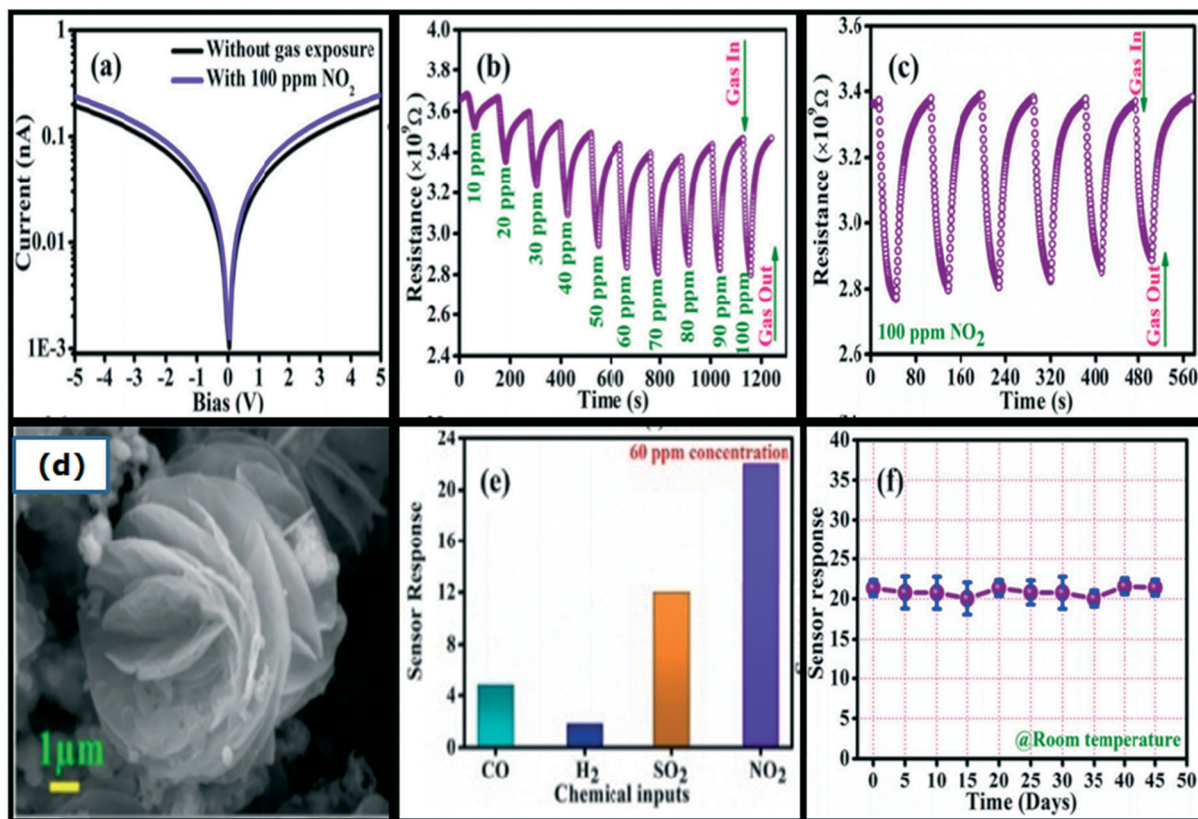
Fig. 7 (a) Log scale I–V curves. Resistance response during cyclic exposure at (b) different and (c) fixed concentrations. Sensor response *versus* (d) Co_3O_4 FESEM and (e) different chemical inputs, and (f) stability of the sensor at RT.[105]

5.1 Metal-doped NMOS-based NO_2 gas sensors

The gas-sensing performance of NO_2 gas sensors has also been improved by the doping of noble metals, such as Pd,[106,107] Au (ref. 108 and 109) and Ag,[110] and metal ions, such as Al^{3+},[101] Cu^{2+},[111] Sb^{5+} (ref. 96) and Zn^{2+},[112] in MOS. The noble metals are highly active catalysts that produce more oxygen species by adsorbing oxygen molecules, and more oxygen ions are formed on the surface of the MOS. Thus, the gas sensing performance is enhanced. On the other hand, doping with metal ions in MOS can increase the number of active sites and defects on the surface of MOS. Thus, increase in the number of oxygen species and enhancement of the adsorbed gas molecules on the sensor's surface increase the gas sensing performance.

A Pd/ZnO nanoparticles-based Schottky diode gas sensor fabricated by thermal evaporation method showed a high response with a value of ~45.2 and good response/recovery times of 67/250 s for 50 ppm NO_2 at RT.[106]

The Au-loaded SnO_2 thin film was prepared using DC/RF sputtering and heat-treated at 600 °C in argon (Ar) atmosphere for the duration of 1 h. Fig. 6(a) shows the SEM images, while the response-recovery curves of the sensor in various concentrations of NO_2 are shown in Fig. 6(b). The graph between the response and response time at different operating temperatures is shown in Fig. 6(c). The sensor

shows good selectivity compared to the other gases, including H_2, CO_2, NH_3, and C_4H_{10}, as shown in Fig. 6(d).[113] The sensor revealed a good response with a value of 90 and a fast response time (70 s) towards 50 ppm NO_2 at RT compare to pure Au and SnO_2 film-based sensors. The high performance of the sensor can be ascribed to the efficient dispersion of Au-nanoparticles over SnO_2 films. In this study, it was observed that the gold nanoparticles acted as the catalyst leading to oxygen dissociation, which facilitated the adsorption of oxygen ions, as shown in Fig. 6(e), while the extraction of more electrons from the conduction band is shown in Fig. 6(f), due to which the sensing response property improved.[113]

The Al/NiO-based gas sensor prepared by solvent-thermal technique exhibited fast response/recovery time (50/200 s) and very low LOD of the value of 250 ppb towards NO_2.[101] The response value of the Al/NiO sensor is 19.66 to 10 ppm of NO_2 at RT, which is higher than that of pure NiO (0.56). This enhancement of the response value can be attributed to the increased oxygen vacancies after Al^{3+} doping.[101]

5.2 Carbon NMOS-based NO_2 gas sensors

The NO_2 gas sensing performance of MOS can be improved by combining them with other metal oxides or carbon-based nanomaterials. The sensor-based on CuO/rGO nanohybrid

nanosheets fabricated by the hydrothermal method can detect a very low concentration of NO_2 (60 ppb) with a good sensitive response (18 to 1 ppm NO_2).[114] The sensor presented a fast response/recovery time (66/34 s) and high stability for sensing down to 5 ppm NO_2. This CuO/rGO heterojunction-based sensor was also found to be very selective towards NO_2 against various interfering gases, such as CO_2, SO_2, and HCHO.[114] CuO nanoflakes modified with rGO nanosheets (CuO/rGO) were synthesized by using a cost-effective hydrothermal method with thermal treatment. The synthesized composite CuO/rGO-based sensor showed a high response behavior of ~400.8% towards 5 ppm NO_2 gas with good stability (30 days) and reliable repeatability.[115] SnO_2/rGO-based sensors showed good sensing performance towards NO_2 gas with a fast response (12 s) and recovery time (34 s), as well as good selectivity and repeatability. The enhancement in the sensing performance was observed due to the synergistic effect of SnO_2 and rGO.[116]

5.3 Composites and MOS heterostructures-based NO_2 gas sensors

Various composite nanomaterials, such as, NiO/SnO_2,[102] ZnO/rGO,[117] CuO/rGO,[114] In_2O_3/SnO_2,[118] In_2O_3/TiO_2,[119] ZnO/SnO_2,[120] and SnO_2/rGO,[121,122] and their sensing parameters are also listed in Table 2. The NO_2 sensor-based In_2O_3-composited SnO_2 nanorod heterostructures were prepared using the electrospinning method.[118] The sensor exhibits remarkable response times of 4.67 s and LOD as low as 0.1 ppm at RT, and showed a response value of (8.98) for 100 ppm NO_x, which was 11 times higher than that of pure SnO_2 nanorods.

The ZnO/SnO_2 composites (with a Zn and Sn molar ratio of 1:1) were prepared by hydrolyzing $SnCl_2$ on ZnO nanorods using the wet chemical method. The ZnO/SnO_2 composite nanomaterials-based sensors showed an excellent response value of 1266 to 0.5 ppm NO_2 at RT and a low LOD of ~200 ppb.[120]

Recent investigations demonstrated that heterojunction structures of various materials could be a good candidate for gas sensors as they improved the gas sensing performances by charge transfer effects. Especially, graphene-based metal oxide heterojunction structures are emerging as the best candidates for gas sensing operations because they have high mobility carriers to enhance the charge transfer effects.[123]

Liu et al. reported the enhancement in NO_2 gas sensing performance by ZnO/rGO nano composite heterojunction structures. The ZnO nanowalls were vertically grown on the rGO thin film using a soft solution process to obtain a heterojunction structure. The ZnO/rGO nanocomposite-based sensor showed a higher response of 9.61 and fast response/recovery speeds of 25/15 s to 50 ppm NO_2 at RT. The improvement in these sensing properties was observed due to the 3D network of planar rGO sheets and porous structure of ZnO nanowalls, and a strong connection between the ZnO nanowalls and rGO.[117] A similar study on the SnO_2/rGO

hybrid composite-based NO_2 sensing film was carried out by Zhang et al.[122] using the hydrothermal method, in which SnO_2 nanocrystals were attached on the surface of the rGO sheets. The SnO_2/rGO hybrid composite sensor exhibits a higher response value than the pure rGO film sensor towards NO_2. This may be due to the formation of a p–n heterojunction at the interface between rGO and SnO_2. The Fermi energy of rGO is higher than that of SnO_2, so electrons can be transported to SnO_2 from rGO, which can improve the adsorption of NO_2 molecules, resulting in enhanced gas-sensing performance.[122]

A chemically prepared SnO_2–CuO/rGO ternary composite-based sensor showed 8–15 times higher sensing response than those of CuO/rGO towards 50 ppm NO_2. It was observed that the SnO_2–CuO/rGO ternary composite showed a low limit of detection (150 ppb), good selectivity, and long-term stability. These results can be attributed to the synergistic effect and nanostructure nature of the composite.[166] The SnO_2–boron nitride nanotubes-based gas sensor was studied for NO_2 detection.[173] A design of a MOS-based (SnO_2–BNNTs) sensing device is shown in Fig. 8. A thin film of BNNTs was coated onto the sensor platform by a spin coating process. Furthermore, SnO_2 was deposited on the surface of BNNT by the RF-sputtering technique. Pt wire electrodes were connected with the help of a silver paste for making the NO_2 sensor device (shown in Fig. 8).

The response/recovery times were studied by exposure of varied NO_2 concentrations from 250 ppb to 5 ppm at different operating temperatures (25–300 °C). The SnO_2–BNNTs sensor showed good selectivity and a maximum response of ~2610 towards 5 ppm NO_2 at low operating temperature.

Fig. 9(a) shows the morphology of the as-developed sensor, and the gas response towards NO_2 can be seen in Fig. 9(b). Fig. 9(c) shows the change in resistance of the sensor to 5 ppm of various target gases (hydrogen, benzene, ethanol, carbon monoxide, and nitrogen dioxide) at optimal operating temperature. The sensor showed the highest sensor response towards NO_2 gas and lower response to other interfering gases. This was due to the modulation of the space charge depletion layer at the p–n heterojunction, which encouraged the tunneling effect by the trapping of NO_2 molecules and offered conducted channels through BNNTs to charge carriers at low operating temperatures (shown in Fig. 9(d)).[173]

In addition to the MOS sensing technique, several other detection techniques are available for NO_2 detection, such as optical, photoacoustic, gas chromatographic methods, and chemiluminescence. Although these sensing techniques provide good sensitivity, selectivity, and limit of detection, the large size and high cost of these conventional gas detectors, such as gas chromatography–mass spectrometry (GC–MS), Fourier transform infrared (FT-IR) and photoacoustic spectrometry, restrict their usage for portable applications. On the other hand, NMOS-based gas sensors are compact, portable, and cost-effective. Therefore, NMOS-
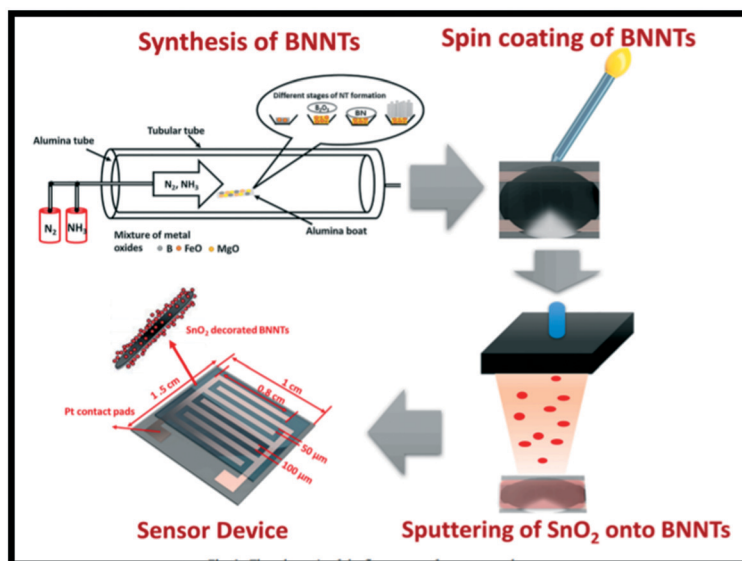
Fig. 8 The schematic of the flow process for the SnO$_2$–BNNTs sensor.[173]

based sensors can be a suitable replacement for these technologies.

Thus, the monitoring of NO$_2$ gas from the environment is necessary. Therefore, the development of an efficient sensing technology is extremely important. The above review and Table 2 summarize the outcome of various research studies for the detection of NO$_2$ gas using a wide range of materials and a variety of synthesis methods. The composite materials
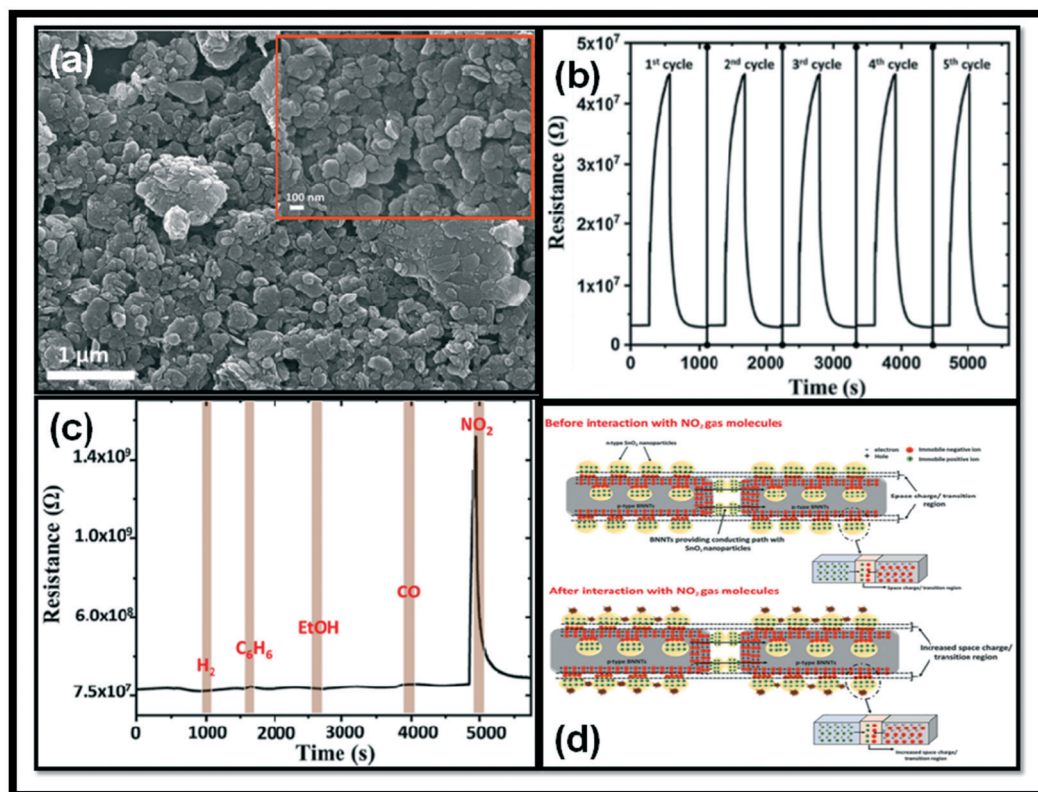
Fig. 9 (a) FESEM image of SnO$_2$–BNNTs; inset shows the enlarged view. (b) Gas responses of the sensor for 5 cycles to 250 ppb NO$_2$ at 100 °C. (c) Change in resistance of the sensor towards 5 ppm of various target gases (hydrogen, benzene, ethanol, carbon monoxide, and nitrogen dioxide) at 100 °C, (d). Variation of the space charge region at the interface of the n-type SnO$_2$ and p-type BNNTs–SnO$_2$ in the absence and presence of the NO$_2$ target gas.[173]

consisting of MOS as one of the components are highly promising candidates to be used as practical NO_2 gas sensors because of their high response, fast response/recovery time, and high repeatability and durability.

6. Fabrication of NMOS–based NO_2 gas sensors

The NMOS-based NO_2 gas sensors are fabricated by direct growth of MOS nanostructures on the substrate material through ultrasonic spray pyrolysis,[20] thermal evaporation,[106,174] CVD,[130] electrospinning,[118] PLD,[92] magnetron sputtering,[137] microwave synthesis,[101] lithography and thermal evaporation.[174] A different process for the manufacturing of MOS-nanostructured NO_2 gas sensors is pre-synthesis, followed by deposition (using spin coating, paste printing, and PLD methods) of the as-prepared MOS-based nanomaterials synthesized by hydrothermal,[19,102,103,125,126] solvothermal,[135] sol–gel,[106,136] and others.[175,176]

An easy process for the fabrication of a MOS-based nanomaterials sensor for the detection of NO_2 gas is pelletization. In this approach, MOS nanomaterials are pressed into a pellet with the desired diameters and thicknesses under a high pressure of ~10 MPa. An appropriate adhesive agent such as ethanol is mixed and ground prior to pressing the MOS material to make a pellet. Soldering wires (Au and Pt) are soldered on both sides of the prepared pellet using Au and Ag paste to shape a sensor constituent.[175]

In addition to these methods, micro-electromechanical systems (MEMS) NO_2 gas sensors are mostly designed on metal oxides. MEMS-based gas sensors are trendy and have several advantages, such as their compact size, good repeatability, good mechanical stability, and low power expenditure, and they are well-suited for wearable applications.[177] In MEMS, the design of the sensing device is started on a wafer. The wafer is then decorated using the photo-lithography process for heater configuration, followed by electrode deposition using physical vapor deposition (thermal and e-beam evaporation methods). In the next step, the micro-heaters are isolated using a passivation layer like Si_3N_4 by lithography and reactive ion etching. Furthermore, inter-digitated-electrodes (IDE) are patterned on wafers by lithography, followed by Pt coating and lift-off process. The sensing area is also defined using a layer of MOS-based nanostructures on the device by lithography, followed by deposition and lift-off processes.[178]

The excess concentration of NO_2 gas is a great challenge for agriculture practices. The concentration of NO_2 gas in the atmosphere/ecosystem should be monitored smartly for intelligent agricultural applications for high crop yield, and this can only be possible with the design of smart metal oxide-based NO_2 sensors.

The MOS-based NO_2 gas sensors applications mainly include the refinement of air quality equally in indoor and outdoor environments. MOS-based NO_2 sensors have significant down-streaming applications in various areas such as commercial areas, pesticides, and insecticides in the agricultural sector.

7. Conclusions

With its high concentration, nitrogen dioxide (NO_2) is one of the harmful and widespread air pollutants for human health, as well as to the plant ecosystem. The excess NO_2 in the ambient air can tarnish the plants in several ways by deteriorating their leaves, limiting their overall growth, and capitulating several crops. To prevent the ecosystem from this harm, the precise monitoring of NO_2 gas levels in the atmosphere/ecosystem is needed for high crop yield. The NMOS-based sensors are found to be more appropriate in terms of their low cost, robustness, LOD, accuracy, long lifetime and wide range of target gases compared to other sensing techniques. MOS and its composites consisting of the rGO and catalyst (Pd, Pt, Au) with nanorods/nanowires morphology have been found to have excellent sensing characteristics for NO_2 gas.

Until now, NMOS-based sensors detect NO_2 gas in a few seconds. Therefore, designing NO_2 gas sensors with a response time of a few milliseconds or microseconds is still challenging. The approach to pick up the ultrafast sensors depends mostly on the interconnection between the NO_2 gas molecules and the surface of the sensing layer, and the transportation of charge in MOS. The fast transfer of charge in sensing devices based on MOS heterostructures can provide a notable improvement in the response and recovery time. In addition, light-assisted MOS-based NO_2 sensors have opened a new way to design fast, reversible and room temperature-operated NO_2 sensors. Thermal isolation in integrated circuits is essential to overcome the high operating temperature challenge in MOS-based sensors. Environmental conditions, such as temperature, humidity, corrosion, residual charges, and poisonous vapor, significantly decrease the strength, consistency, and repeatability of the NO_2 gas sensors. The excellent selectivity and repeatability with no drift fault owing to age and environment are still big challenges for researchers. Efforts are necessary to conquer the challenges of MOS-based NO_2 gas sensors, and to manufacture capable and trustworthy sensor devices for their use in the agriculture field and real-life applications. A more efficient and suitable NMOS-based sensor can be designed by doping, organic sensitization, inorganic heterojunction, and oxygen vacancy modification.

CRediT authorship contribution statement

Shrestha Tyagi: writing – original draft, methodology, data curation. Manika Chaudhary: investigation, formal analysis, software. Anit K. Ambedkar: investigation, preparation. Kavita Sharma: writing – review & editing, conceptualization, visualization, validation. Yogendra K. Gautam: writing –

conceptualization, review & editing, supervision. Beer Pal Singh: supervision, resources, conceptualization, funding acquisition.

Conflicts of interest

The authors have no conflicts of interest to declare.

Acknowledgements

References

1 WHO, *Effects of nitrogen containing air pollutants: critical levels, Air Qual. Guidel. Eur.*, 2nd edn, 2000, p. 288.

2 Nitrogen Oxides (NOx), Why and How They Are Controlled, 1999, http://www.epa.gov/ttn/catc (accessed May 23, 2021).

3 R. B. R. B. R. S. Dorice Price, &EPA Stratospheric Ozone Depletion Global Warming Toxic Products Nitrogen Oxides: Impacts on Public Health and the Environment Ozone, Particulate Matter, and Nitrogen Dioxide Acid Deposition Visibility, Drinking Water and Ecosystem Protection Eutrophicati, 1997, 1–161, https://nepis.epa.gov/Exe/ZyNET. exe/2000DM8Q.txt?ZyActionD=ZyDocument&Client= EPA&Index=1995 Thru 1999&Docs=&Query=&Time= &EndTime=&SearchMethod=1&TocRestrict=n&Toc= &TocEntry=&QField=&QFieldYear=&QFieldMonth= &QFieldDay=&UseQField=&IntQFieldOp=0&ExtQFieldOp=.

4 I. Florentina and B. Io, The Effects of Air Pollutants on Vegetation and the Role of Vegetation in Reducing Atmospheric Pollution, in *Impact Air Pollut. Heal. Econ. Environ. Agric. Sources*, InTech, 2011, DOI: 10.5772/17660.

5 A. A. Al-Jalal, W. Al-Basheer, K. Gasmi and M. S. Romadhon, Measurement of low concentrations of NO2 gas by differential optical absorption spectroscopy method, *Meas.: J. Int. Meas. Confed.*, 2019, **146**, 613–617, DOI: 10.1016/j.measurement.2019.07.022.

6 T. Rück, R. Bierl and F. M. Matysik, Low-cost photoacoustic NO2 trace gas monitoring at the pptV-level, *Sens. Actuators, A*, 2017, **263**, 501–509, DOI: 10.1016/j.sna.2017.06.036.

7 J. S. Gaffney, R. M. Bornick, Y. H. Chen and N. A. Marley, Capillary gas chromatographic analysis of nitrogen dioxide and pans with luminol chemiluminescent detection, *Atmos. Environ.*, 1998, 1445–1454, DOI: 10.1016/S1352-2310(97)00098-8.

8 C. Zhang, Y. Luo, J. Xu and M. Debliquy, Room temperature conductive type metal oxide semiconductor gas sensors for NO 2 detection, *Sens. Actuators, A*, 2019, **289**, 118–133, DOI: 10.1016/j.sna.2019.02.027.

9 J. Zhang, Z. Qin, D. Zeng and C. Xie, Metal-oxide-semiconductor based gas sensors: Screening, preparation, and integration, *Phys. Chem. Chem. Phys.*, 2017, **19**, 6313–6329, DOI: 10.1039/c6cp07799d.

10 S. Kumar, V. Pavelyev, N. Tripathi, V. Platonov, P. Sharma, R. Ahmad, P. Mishra and A. Khosla, Review—Recent Advances in the Development of Carbon Nanotubes Based Flexible Sensors, *J. Electrochem. Soc.*, 2020, **167**, 047506, DOI: 10.1149/1945-7111/AB7331.

11 S. Kumar, V. Pavelyev, P. Mishra and N. Tripathi, Thin film chemiresistive gas sensor on single-walled carbon nanotubes-functionalized with polyethylenimine (PEI) for NO 2 gas sensing, *Bull. Mater. Sci.*, 2034, **43**, 61, DOI: 10.1007/s12034-020-2043-6.

12 A. Dey, Semiconductor metal oxide gas sensors: A review, *Mater. Sci. Eng. B: Solid-State Mater. Adv. Technol.*, 2018, **229**, 206–217, DOI: 10.1016/j.mseb.2017.12.036.

13 B. Saruhan, R. L. Fomekong and S. Nahirniak, Review: Influences of Semiconductor Metal Oxide Properties on Gas Sensing Characteristics, *Front. Sens.*, 2021, 2, DOI: 10.3389/FSENS.2021.657931.

14 J. Xuan, G. Zhao, M. Sun, F. Jia, X. Wang, T. Zhou, G. Yin and B. Liu, Low-temperature operating ZnO-based NO 2 sensors: a review, *RSC Adv.*, 2020, **10**, 39786–39807, DOI: 10.1039/D0RA07328H.

15 I. Muniyandi, G. K. Mani, P. Shankar and J. B. B. Rayappan, Effect of nickel doping on structural, optical, electrical and ethanol sensing properties of spray deposited nanostructured ZnO thin films, *Ceram. Int.*, 2014, **40**, 7993–8001, DOI: 10.1016/J.CERAMINT.2013.12.150.

16 Y. K. Gautam, K. Sharma, S. Tyagi, A. K. Ambedkar, M. Chaudhary and B. Pal Singh, Nanostructured metal oxide semiconductor-based sensors for greenhouse gas detection: progress and challenges, *R. Soc. Open Sci.*, 2021, **8**, 201324, DOI: 10.1098/rsos.201324.

17 H. Ji, W. Zeng and Y. Li, Gas sensing mechanisms of metal oxide semiconductors: A focus review, *Nanoscale*, 2019, **11**, 22664–22684, DOI: 10.1039/c9nr07699a.

18 C. Wang, L. Yin, L. Zhang, D. Xiang and R. Gao, Metal Oxide Gas Sensors: Sensitivity and Influencing Factors, *Sensors*, 2010, **10**, 2088–2106, DOI: 10.3390/S100302088.

19 J. Gao, H. Wu, J. Zhou, L. Yao, G. Zhang, S. Xu, Y. Xie, L. Li and K. Shi, Mesoporous In2O3 nanocrystals: Synthesis, characterization and NOx gas sensor at room temperature, *New J. Chem.*, 2016, **40**, 1306–1311, DOI: 10.1039/c5nj02214b.

20 T. Hyodo, H. Inoue, H. Motomura, K. Matsuo, T. Hashishin, J. Tamaki, Y. Shimizu and M. Egashira, NO2 sensing properties of macroporous In2O 3-based powders fabricated by utilizing ultrasonic spray pyrolysis employing polymethylmethacrylate microspheres as a template, *Sens. Actuators, B*, 2010, **151**, 265–273, DOI: 10.1016/j.snb.2010.09.002.

21 E. F. Darley, Vegetation Damage from Air Pollution, in *Combust. Air Pollut.*, Springer US, 1971, pp. 245–255, DOI: 10.1007/978-1-4684-7574-6_10.

22 T. Nakaji, M. Fukami, Y. Dokiya and T. Izuta, Effects of high nitrogen load on growth, photosynthesis and nutrient status of Cryptomeria japonica and Pinus densiflora seedlings, *Trees - Struct. Funct.*, 2001, **15**, 453–461, DOI: 10.1007/s00468-001-0130-x.

23 A. J. Zeevaart, Some effects of fumigating plants for short periods with NO2, *Environ. Pollut.*, 1976, **11**, 97–108, DOI: 10.1016/0013-9327(76)90022-7.

24 K. Okano and T. Totsuka, Absorption of nitrogen dioxide by sunflower plants grown at various levels of nitrate, *New Phytol.*, 1986, **102**, 551–562, DOI: 10.1111/j.1469-8137.1986.tb00831.x.

25 P. Schmutz, D. Tarjan, M. S. Günthardt-Goerg, R. Matyssek and J. B. Bucher, Nitrogen Dioxide-a Gaseous Fertilizer of Poplar Trees, *Phyton (Horn, Austria)*, 1995, **35**, 219–232.

26 F. Ferrini, A. Fini, J. Mori and A. Gori, Role of vegetation as a mitigating factor in the urban context, *Sustain*, 2020, **12**(10), 4247, DOI: 10.3390/su12104247.

27 J. Li, C. Yin, H. Chen and G. Lei, Response and relative resistance of green plants to NO2 injury, *Yuanyi Xuebao*, 1982, **9**, 57–63, (in Chinese).

28 Q. Sheng and Z. Zhu, Effects of nitrogen dioxide on biochemical responses in 41 garden plants, *Plants*, 2019, **8**(2), 45, DOI: 10.3390/plants8020045.

29 Z. M. Chen, Y. X. Chen, G. J. Du, X. L. Wu and F. Li, Effects of 60-day NO2 fumigation on growth, oxidative stress and antioxidative response in Cinnamomum camphora seedlings, *J. Zhejiang Univ., Sci., B*, 2010, **11**, 190–199, DOI: 10.1631/jzus.B0910350.

30 Y. Hu, N. Bellaloui, M. Tigabu, J. Wang, J. Diao, K. Wang, R. Yang and G. Sun, Gaseous NO2 effects on stomatal behavior, photosynthesis and respiration of hybrid poplar leaves, *Acta Physiol. Plant.*, 2015, **37**, DOI: 10.1007/s11738-014-1749-8.

31 Q. Sheng and Z. Zhu, Photosynthetic capacity, stomatal behavior and chloroplast ultrastructure in leaves of the endangered plant Carpinus putoensis W.C. Cheng during Gaseous NO2 exposure and after recovery, *Forests*, 2018, **9**, 561, DOI: 10.3390/f9090561.

32 Nitrogen oxide, (n.d.). http://www.nbrienvis.nic.in/Database/1_2039.aspx (accessed May 23, 2021).

33 J. G. Firth, A. Jones and T. A. Jones, The principles of the detection of flammable atmospheres by catalytic devices, *Combust. Flame*, 1973, **20**, 303–311, DOI: 10.1016/0010-2180(73)90021-7.

34 J. R. Bates and M. Campbell, Gas sensors and analysers, in *Sens. Syst. Environ. Monit.*, Springer Netherlands, 1997, pp. 127–178, DOI: 10.1007/978-94-009-1571-8_5.

35 K. U. Leuven, F. Ingenieurswetenschappen, D. Werktuigkunde, A. T. Mechanica and E. N. Energieconversie, *Influence of Process Conditions on the Auto-Ignition Temperature of*, 2008.

36 Z. Yunusa, M. N. Hamidon, A. Kaiser and Z. Awang, Gas Sensors: A Review, *Sens. Transducers J.*, 2014, **168**(4), 61–75.

37 R. Laref, E. Losson, A. Sava and M. Siadat, Empiric Unsupervised Drifts Correction Method of Electrochemical Sensors for in Field Nitrogen Dioxide Monitoring, *Sensors*, 2021, **21**, 3581, DOI: 10.3390/S21113581.

38 J. Fraden, *Handbook of modern sensors: Physics, designs, and applications*, Springer International Publishing, 2016, DOI: 10.1007/978-3-319-19303-8.

39 A. Paliwal, A. Sharma, M. Tomar and V. Gupta, Room temperature detection of NO2 gas using optical sensor based on surface plasmon resonance technique, *Sens. Actuators, B*, 2015, **216**, 497–503, DOI: 10.1016/j.snb.2015.03.095.

40 J. Huang and Q. Wan, Gas sensors based on semiconducting metal oxide one-dimensional nanostructures, *Sensors*, 2009, **9**, 9903–9924, DOI: 10.3390/s91209903.

41 M. Li, H. Kan, S. Chen, X. Feng, H. Li, C. Li, C. Fu, A. Quan, H. Sun, J. Luo, X. Liu, W. Wang, H. Liu, Q. Wei and Y. Fu, Colloidal quantum dot-based surface acoustic wave sensors for NO2-sensing behavior, *Sens. Actuators, B*, 2019, **287**, 241–249, DOI: 10.1016/J.SNB.2019.02.042.

42 G. Galán, M. J. Navas and A. M. Jiménez, Determination of sulfur compounds in air by chemiluminescence, *Int. J. Environ. Anal. Chem.*, 1997, **68**, 497–510, DOI: 10.1080/03067319708030849.

43 L. Zhang, J. Hu, Y. Lv and X. Hou, Recent progress in chemiluminescence for gas analysis, *Appl. Spectrosc. Rev.*, 2010, **45**, 474–489, DOI: 10.1080/05704928.2010.503527.

44 Metal Oxide Gas Sensing Material and MEMS Process | FierceElectronics, (n.d.). https://www.fierceelectronics.com/components/metal-oxide-gas-sensing-material-and-mems-process (accessed July 19, 2021).

45 Nitrogen Dioxide Sensors | NO2 Gas Detectors | Alphasense, (n.d.). https://www.alphasense.com/products/nitrogen-dioxide/ (accessed July 19, 2021).

46 Catalytic gas sensor - Dräger Safety - hydrogen, (n.d.). https://www.directindustry.com/prod/draeger-safety/product-20351-450012.html (accessed July 19, 2021).

47 A. G. Bell, On the production and reproduction of sound by light, *Am. J. Sci.*, 1880, **s3–s20**, 305–324, DOI: 10.2475/ajs.s3-20.118.305.

48 F. J. M. Harren and S. M. Cristescu, Photoacoustic Spectroscopy in Trace Gas Monitoring, in *Encycl. Anal. Chem.*, Wiley, 2019, pp. 1–29, DOI: 10.1002/9780470027318.a0718.pub3.

49 J. Peltola, T. Hieta and M. Vainio, Parts-per-trillion-level detection of nitrogen dioxide by cantilever-enhanced photo-acoustic spectroscopy, *Opt. Lett.*, 2015, **40**, 2933, DOI: 10.1364/OL.40.002933.

50 A. V. Nikam, B. L. V. Prasad and A. A. Kulkarni, Wet chemical synthesis of metal oxide nanoparticles: A review, *CrystEngComm*, 2018, **20**, 5091–5107, DOI: 10.1039/C8CE00487K.

51 M. S. Chavali, M. P. Nikolova and A. Silver, Metal oxide nanoparticles and their applications in nanotechnology, *SN Appl. Sci.*, 2019, **1**, 1–30, DOI: 10.1007/s42452-019-0592-3.

52 Y. F. Sun, S. B. Liu, F. L. Meng, J. Y. Liu, Z. Jin, L. T. Kong and J. H. Liu, Metal oxide nanostructures and their gas sensing properties: A review, *Sensors*, 2012, **12**, 2610–2631, DOI: 10.3390/s120302610.

53 Z. Sun, T. Liao and L. Kou, Strategies for designing metal oxide nanostructures, *Sci. China Mater.*, 2017, **60**, 1–24, DOI: 10.1007/s40843-016-5117-0.

54 Y. F. Sun, S. B. Liu, F. L. Meng, J. Y. Liu, Z. Jin, L. T. Kong and J. H. Liu, Metal oxide nanostructures and their gas sensing properties: A review, *Sensors*, 2012, **12**, 2610–2631, DOI: 10.3390/s120302610.

55 L. Li, C. Zhang and W. Chen, Fabrication of SnO2–SnO nanocomposites with p–n heterojunctions for the low-temperature sensing of NO2 gas, *Nanoscale*, 2015, **7**, 12133–12142, DOI: 10.1039/C5NR02334C.

56 X. Xin, Y. Zhang, X. Guan, J. Cao, W. Li, X. Long and X. Tan, Enhanced Performances of PbS Quantum-Dots-Modified MoS2 Composite for NO2 Detection at Room Temperature, *ACS Appl. Mater. Interfaces*, 2019, **11**, 9438–9447, DOI: 10.1021/ACSAMI.8B20984.

57 A. Labidi, E. Gillet, R. Delamare, M. Maaref and K. Aguir, Ethanol and ozone sensing characteristics of WO3 based sensors activated by Au and Pd, *Sens. Actuators, B*, 2006, **120**, 338–345, DOI: 10.1016/j.snb.2006.02.015.

58 P. P. Sahay, S. Tewari, S. Jha and M. Shamsuddin, Sprayed ZnO thin films for ethanol sensors, *J. Mater. Sci.*, 2005, **40**, 4791–4793, DOI: 10.1007/s10853-005-0519-9.

59 T. V. Belysheva, L. P. Bogovtseva, E. A. Kazachkov and N. V. Serebryakova, Gas-Sensing Properties of Doped In2O3 Films as Sensors for NO2 in Air, *J. Anal. Chem.*, 2003, **58**, 583–587, DOI: 10.1023/A:1024176505338.

60 A. Z. Sadek, S. Choopun, W. Wlodarski, S. J. Ippolito and K. Kalantar-Zadeh, Characterization of ZnO Nanobelt-Based Gas Sensor for H2, NO2, and Hydrocarbon Sensing, *IEEE Sens. J.*, 2007, **7**, 919–924, DOI: 10.1109/JSEN.2007.895963.

61 B. Shouli, C. Liangyuan, L. Dianqing, Y. Wensheng, Y. Pengcheng, L. Zhiyong, C. Aifan and C. C. Liu, Different morphologies of ZnO nanorods and their sensing property, *Sens. Actuators, B*, 2010, **146**, 129–137, DOI: 10.1016/j.snb.2010.02.011.

62 N. Yamazoe and N. Miura, New Approaches in the Design of Gas Sensors, *Gas Sens.*, 1992, 1–42, DOI: 10.1007/978-94-011-2737-0_1.

63 J. Gong, Q. Chen, M. R. Lian, N. C. Liu, R. G. Stevenson and F. Adami, Micromachined nanocrystalline silver doped SnO2 H2S sensor, *Sens. Actuators, B*, 2006, **114**, 32–39, DOI: 10.1016/j.snb.2005.04.035.

64 C. Zhang, M. Debliquy, A. Boudiba, H. Liao and C. Coddet, Sensing properties of atmospheric plasma-sprayed WO3 coating for sub-ppm NO2 detection, *Sens. Actuators, B*, 2010, **144**, 280–288, DOI: 10.1016/j.snb.2009.11.006.

65 D. Meng, T. Yamazaki, Y. Shen, Z. Liu and T. Kikuta, Preparation of WO 3 nanoparticles and application to NO2 sensor, *Appl. Surf. Sci.*, 2009, **256**, 1050–1053, DOI: 10.1016/j.apsusc.2009.05.075.

66 M. Penza, C. Martucci and G. Cassano, NOx gas sensing characteristics of WO3 thin films activated by noble metals (Pd, Pt, Au) layers, *Sens. Actuators, B*, 1998, **50**, 52–59, DOI: 10.1016/S0925-4005(98)00156-7.

67 L. Chen and S. C. Tsang, Ag doped WO3-based powder sensor for the detection of NO gas in air, *Sens. Actuators, B*, 2003, **89**, 68–75, DOI: 10.1016/S0925-4005(02)00430-6.

68 J. Herrán, G. Ga Mandayo and E. Castaño, Semiconducting BaTiO3-CuO mixed oxide thin films for CO2 detection, *Thin Solid Films*, 2009, **517**, 6192–6197, DOI: 10.1016/j.tsf.2009.04.007.

69 L. A. Patil, M. D. Shinde, A. R. Bari and V. V. Deo, Highly sensitive and quickly responding ultrasonically sprayed nanostructured SnO2 thin films for hydrogen gas sensing, *Sens. Actuators, B*, 2009, **143**, 270–277, DOI: 10.1016/j.snb.2009.09.048.

70 Y. Min, H. L. Tuller, S. Palzer, J. Wöllenstein and H. Böttner, Gas response of reactively sputtered ZnO films on Si-based micro-array, *Sens. Actuators, B*, 2003, **93**(1–3), 435–441, DOI: 10.1016/S0925-4005(03)00170-9.

71 V. Srivastava and K. Jain, Highly sensitive NH3 sensor using Pt catalyzed silica coating over WO3 thick films, *Sens. Actuators, B*, 2008, **133**, 46–52, DOI: 10.1016/j.snb.2008.01.066.

72 S. Das, S. Chakraborty, O. Parkash, D. Kumar, S. Bandyopadhyay, S. K. Samudrala, A. Sen and H. S. Maiti, Vanadium doped tin dioxide as a novel sulfur dioxide sensor, *Talanta*, 2008, **75**, 385–389, DOI: 10.1016/j.talanta.2007.11.010.

73 N. J. Dayan, S. R. Sainkar, R. N. Karekar and R. C. Aiyer, Formulation and characterization of ZnO:Sb thick-film gas sensors, *Thin Solid Films*, 1998, **325**, 254–258, DOI: 10.1016/S0040-6090(98)00501-X.

74 A. Friedberger, P. Kreisl, E. Rose, G. Müller, G. Kühner, J. Wöllenstein and H. Böttner, Micromechanical fabrication of robust low-power metal oxide gas sensors, *Sens. Actuators, B*, 2003, 345–349, DOI: 10.1016/S0925-4005(03)00221-1.

75 A. Teleki, N. Bjelobrk and S. E. Pratsinis, Flame-made Nb- and Cu-doped TiO2 sensors for CO and ethanol, *Sens. Actuators, B*, 2008, **130**, 449–457, DOI: 10.1016/j.snb.2007.09.008.

76 Electrode effects on gas sensing properties of nanocrystalline zinc oxide - ScienceDirect, (n.d.). https://www.sciencedirect.com/science/article/abs/pii/S0965977398000877 (accessed May 23, 2021).

77 B. Karunagaran, P. Uthirakumar, S. J. Chung, S. Velumani and E. K. Suh, TiO2 thin film gas sensor for monitoring ammonia, *Mater. Charact.*, 2007, **58**, 680–684, DOI: 10.1016/j.matchar.2006.11.007.

78 N. V. Hieu, L. T. B. Thuy and N. D. Chien, Highly sensitive thin film NH3 gas sensor operating at room temperature based on SnO2/MWCNTs composite, *Sens. Actuators, B*, 2008, **129**, 888–895, DOI: 10.1016/J.SNB.2007.09.088.

79 J. Xu, X. Wang and J. Shen, Hydrothermal synthesis of In2O3 for detecting H2S in air, *Sens. Actuators, B*, 2006, **115**, 642–646, DOI: 10.1016/j.snb.2005.10.038.

80 L. Mädler, T. Sahm, A. Gurlo, J. D. Grunwaldt, N. Barsan, U. Weimar and S. E. Pratsinis, Sensing low concentrations of CO using flame-spray-made Pt/SnO2 nanoparticles, *J. Nanopart. Res.*, 2006, **8**, 783–796, DOI: 10.1007/s11051-005-9029-6.

81 T. Wagner, T. Waitz, J. Roggenbuck, M. Fröba, C. D. Kohl and M. Tiemann, Ordered mesoporous ZnO for gas sensing, *Thin Solid Films*, 2007, **515**, 8360–8363, DOI: 10.1016/j.tsf.2007.03.021.

82 C. M. Ghimbeu, M. Lumbreras, J. Schoonman and M. Siadat, Electrosprayed metal oxide semiconductor films for sensitive and selective detection of hydrogen sulfide, *Sensors*, 2009, **9**, 9122–9132, DOI: 10.3390/s91109122.

83 J. Riu, A. Maroto and F. X. Rius, Nanosensors in environmental analysis, *Talanta*, 2006, 288–301, DOI: 10.1016/j.talanta.2005.09.045.

84 O. Lupan, V. V. Ursaki, G. Chai, L. Chow, G. A. Emelchenko, I. M. Tiginyanu, A. N. Gruzintsev and A. N. Redkin, Selective hydrogen gas nanosensor using individual ZnO nanowire with fast response at room temperature, *Sens. Actuators, B*, 2010, **144**, 56–66, DOI: 10.1016/j.snb.2009.10.038.

85 B. G. Kim, D. G. Lim, J. H. Park, Y. J. Choi and J. G. Park, In-situ bridging of SnO 2 nanowires between the electrodes and their NO 2 gas sensing characteristics, *Appl. Surf. Sci.*, 2011, **257**, 4715–4718, DOI: 10.1016/j.apsusc.2010.12.137.

86 K. Arshak, E. Moore, G. M. Lyons, J. Harris and S. Clifford, A review of gas sensors employed in electronic nose applications, *Sens. Rev.*, 2004, **24**, 181–198, DOI: 10.1108/02602280410525977.

87 G. Sberveglieri, E. Comini, G. Faglia, M. Z. Atashbar and W. Wlodarski, Titanium dioxide thin films prepared for alcohol microsensor applications, *Sens. Actuators, B*, 2000, **66**, 139–141, DOI: 10.1016/S0925-4005(00)00328-2.

88 Semiconductor Gas Sensors - 1st Edition, (n.d.). https://www.elsevier.com/books/semiconductor-gas-sensors/jaaniso/978-0-85709-236-6 (accessed May 23, 2021).

89 L. Yu, F. Guo, S. Liu, B. Yang, Y. Jiang, L. Qi and X. Fan, Both oxygen vacancies defects and porosity facilitated NO2 gas sensing response in 2D ZnO nanowalls at room temperature, *J. Alloys Compd.*, 2016, **682**, 352–356, DOI: 10.1016/j.jallcom.2016.05.053.

90 X. Pan, X. Zhao, J. Chen, A. Bermak and Z. Fan, A fast-response/recovery ZnO hierarchical nanostructure based gas sensor with ultra-high room-temperature output response, *Sens. Actuators, B*, 2015, **206**, 764–771, DOI: 10.1016/j.snb.2014.08.089.

91 A. M. Andringa, C. Piliego, I. Katsouras, P. W. M. Blom and D. M. D. Leeuw, NO2 detection and real-time sensing with field-effect transistors, *Chem. Mater.*, 2014, **26**, 773–785, DOI: 10.1021/cm4020628.

92 M. Kodu, A. Berholts, T. Kahro, T. Avarmaa, A. Kasikov, A. Niilisk, H. Alles and R. Jaaniso, Highly sensitive NO2 sensors by pulsed laser deposition on graphene, *Appl. Phys. Lett.*, 2016, **109**, 113108, DOI: 10.1063/1.4962959.

93 J. D. Prades, R. Jimenez-Diaz, F. Hernandez-Ramirez, S. Barth, A. Cirera, A. Romano-Rodriguez, S. Mathur and J. R. Morante, Equivalence between thermal and room temperature UV light-modulated responses of gas sensors based on individual SnO2 nanowires, *Sens. Actuators, B*, 2009, **140**, 337–341, DOI: 10.1016/j.snb.2009.04.070.

94 Z. P. Tshabalala, D. E. Motaung, G. H. Mhlongo and O. M. Ntwaeaborwa, Facile synthesis of improved room temperature gas sensing properties of TiO2 nanostructures: Effect of acid treatment, *Sens. Actuators, B*, 2016, **224**, 841–856, DOI: 10.1016/j.snb.2015.10.079.

95 S. J. Kim, I. S. Hwang, J. K. Choi and J. H. Lee, Gas sensing characteristics of WO3 nanoplates prepared by acidification method, *Thin Solid Films*, 2011, **519**, 2020–2024, DOI: 10.1016/j.tsf.2010.10.026.

96 S. Bai, Y. Ma, X. Shu, J. Sun, Y. Feng, R. Luo, D. Li and A. Chen, Doping Metal Elements of WO3 for Enhancement of NO2-Sensing Performance at Room Temperature, *Ind. Eng. Chem. Res.*, 2017, **56**, 2616–2623, DOI: 10.1021/acs.iecr.6b03055.

97 C. Jiang, G. Zhang, Y. Wu, L. Li and K. Shi, Facile synthesis of SnO 2 nanocrystalline tubes by electrospinning and their fast response and high sensitivity to NO x at room temperature, *CrystEngComm*, 2012, **14**, 2739–2747, DOI: 10.1039/c2ce06405g.

98 W. Song, H. Wu, J. Wang, Y. Lin, J. Song, Y. Xie, L. Li and K. Shi, Facile synthesis of hierarchical CuO microspheres and their gas sensing properties for NOx at room temperature, *Aust. J. Chem.*, 2015, **68**, 1569–1576, DOI: 10.1071/CH15126.

99 S. Li, M. Wang, C. Li, J. Liu, M. Xu, J. Liu and J. Zhang, CuxO self-assembled mesoporous microspheres with effective surface oxygen vacancy and their room temperature NO2 gas sensing performance, *Sci. China Mater.*, 2018, **61**, 1085–1094, DOI: 10.1007/s40843-017-9224-x.

100 D. N. Oosthuizen, D. E. Motaung and H. C. Swart, In depth study on the notable room-temperature NO2 gas sensor based on CuO nanoplatelets prepared by sonochemical method: Comparison of various bases, *Sens. Actuators, B*, 2018, **266**, 761–772, DOI: 10.1016/j.snb.2018.03.106.

101 S. Wang, D. Huang, S. Xu, W. Jiang, T. Wang, J. Hu, N. Hu, Y. Su, Y. Zhang and Z. Yang, Two-dimensional NiO nanosheets with enhanced room temperature NO2 sensing performance: Via Al doping, *Phys. Chem. Chem. Phys.*, 2017, **19**, 19043–19049, DOI: 10.1039/c7cp03259e.

102 J. Zhang, D. Zeng, Q. Zhu, J. Wu, Q. Huang and C. Xie, Effect of Nickel Vacancies on the Room-Temperature NO2 Sensing Properties of Mesoporous NiO Nanosheets, *J. Phys. Chem. C*, 2016, **120**, 3936–3945, DOI: 10.1021/acs.jpcc.5b12162.

103 J. Zhang, D. Zeng, Q. Zhu, J. Wu, K. Xu, T. Liao, G. Zhang and C. Xie, Effect of Grain-Boundaries in NiO Nanosheet Layers Room-Temperature Sensing Mechanism under NO2, *J. Phys. Chem. C*, 2015, **119**, 17930–17939, DOI: 10.1021/acs.jpcc.5b04940.

104 X. Zhang, J. Wang, L. Xuan, Z. Zhu, Q. Pan, K. Shi and G. Zhang, Novel Co3O4 nanocrystalline chain material as a high performance gas sensor at room temperature, *J. Alloys Compd.*, 2018, **768**, 190–197, DOI: 10.1016/j.jallcom.2018.07.240.

105 M. Kumar, V. Bhatt and J. H. Yun, Hierarchical 3D micro flower-like Co3O4 structures for NO2 detection at room temperature, *Phys. Lett. A: Gen. At. Solid State Phys.*, 2020, **384**, 126477, DOI: 10.1016/j.physleta.2020.126477.

106 L. Chandra, P. K. Sahu, R. Dwivedi and V. N. Mishra, Electrical and NO2 sensing characteristics of Pd/ZnO nanoparticles based Schottky diode at room temperature, *Mater. Res. Express*, 2017, **4**, 0–17, DOI: 10.1088/2053-1591/aa9cb4.

107 S. Park, H. Kim, C. Jin and C. Lee, Synthesis, structure, and room-temperature gas sensing of multiple-networked Pd-doped Ga 2O 3 nanowires, *J. Korean Phys. Soc.*, 2012, **60**, 1560–1564, DOI: 10.3938/jkps.60.1560.

108 Q. A. Drmosh, A. H. Hendi, M. K. Hossain, Z. H. Yamani, R. A. Moqbel, A. Hezam and M. A. Gondal, UV-activated gold decorated rGO/ZnO heterostructured nanocomposite sensor for efficient room temperature H2 detection, *Sens. Actuators, B*, 2019, **290**, 666–675, DOI: 10.1016/j.snb.2019.03.077.

109 J. Liang, K. Zhu, R. Yang and M. Hu, Room temperature NO2 sensing properties of Au-decorated vanadium oxide nanowires sensor, *Ceram. Int.*, 2018, **44**, 2261–2268, DOI: 10.1016/j.ceramint.2017.10.186.

110 Z. Wang, Y. Zhang, S. Liu and T. Zhang, Preparation of Ag nanoparticles-SnO2 nanoparticles-reduced graphene oxide hybrids and their application for detection of NO2 at room temperature, *Sens. Actuators, B*, 2016, **222**, 893–903, DOI: 10.1016/j.snb.2015.09.027.

111 X. Zou, H. Fan, Y. Tian, M. Zhang and X. Yan, Microwave-assisted hydrothermal synthesis of Cu/Cu2O hollow spheres with enhanced photocatalytic and gas sensing activities at room temperature, *Dalton Trans.*, 2015, **44**, 7811–7821, DOI: 10.1039/c4dt03417a.

112 C. Tao, X. Li, J. Yang and Y. Shi, Optical fiber sensing element based on luminescence quenching of silica nanowires modified with cryptophane-A for the detection of methane, *Sens. Actuators, B*, 2011, **156**, 553–558, DOI: 10.1016/j.snb.2011.01.067.

113 Q. A. Drmosh, Z. H. Yamani, A. K. Mohamedkhair, A. H. Y. Hendi, M. K. Hossain and A. Ibrahim, Gold nanoparticles incorporated SnO2 thin film: highly responsive and selective detection of NO2 at room temperature, *Mater. Lett.*, 2018, **214**, 283–286, DOI: 10.1016/j.matlet.2017.12.013.

114 Z. Li, Y. Liu, D. Guo, J. Guo and Y. Su, Room-temperature synthesis of CuO/reduced graphene oxide nanohybrids for high-performance NO2 gas sensor, *Sens. Actuators, B*, 2018, **271**, 306–310, DOI: 10.1016/j.snb.2018.05.097.

115 H. Bai, H. Guo, J. Wang, Y. Dong, B. Liu, Z. Xie, F. Guo, D. Chen, R. Zhang and Y. Zheng, A room-temperature NO2 gas sensor based on CuO nanoflakes modified with rGO nanosheets, *Sens. Actuators, B*, 2021, **337**, 129783, DOI: 10.1016/j.snb.2021.129783.

116 R. Sivakumar, K. Krishnamoorthi, S. Vadivel and S. Govindasamy, Progress towards a novel NO2 gas sensor based on SnO2/RGO hybrid sensors by a facial hydrothermal approach, *Diamond Relat. Mater.*, 2021, **116**, 108418, DOI: 10.1016/j.diamond.2021.108418.

117 Z. Liu, L. Yu, F. Guo, S. Liu, L. Qi, M. Shan and X. Fan, Facial development of high performance room temperature NO 2 gas sensors based on ZnO nanowalls decorated rGO

nanosheets, *Appl. Surf. Sci.*, 2017, **423**, 721–727, DOI: 10.1016/j.apsusc.2017.06.160.

118 S. Xu, J. Gao, L. Wang, K. Kan, Y. Xie, P. Shen and L. Li, K. S.- Nanoscale, undefined 2015, Role of the heterojunctions in In 2 O 3-composite SnO 2 nanorod sensors and their remarkable gas-sensing performance for NOx at room temperature, Pubs.Rsc.Org. (n.d.). https://pubs.rsc.org/ko/content/articlehtml/2015/nr/c5nr03796d (accessed June 15, 2020).

119 H. Wu, K. Kan, L. Wang, G. Zhang, Y. Yang, H. Li, L. Jing, P. Shen, L. Li and K. Shi, Electrospinning of mesoporous p-type In2O3/TiO2composite nanofibers for enhancing NOxgas sensing properties at room temperature, *CrystEngComm*, 2014, **16**, 9116–9124, DOI: 10.1039/c4ce01248h.

120 G. Lu, J. Xu, J. Sun, Y. Yu, Y. Zhang and F. Liu, UV-enhanced room temperature NO 2 sensor using ZnO nanorods modified with SnO 2 nanoparticles, *Sens. Actuators, B*, 2012, **162**, 82–88, DOI: 10.1016/j.snb.2011.12.039.

121 Z. Wang, T. Zhang, T. Han, T. Fei, S. Liu and G. Lu, Oxygen vacancy engineering for enhanced sensing performances: A case of SnO2 nanoparticles-reduced graphene oxide hybrids for ultrasensitive ppb-level room-temperature NO2 sensing, *Sens. Actuators, B*, 2018, **266**, 812–822, DOI: 10.1016/j.snb.2018.03.169.

122 D. Zhang, J. Liu and B. Xia, Nitrogen Dioxide-Sensing Properties at Room Temperature of Metal Oxide-Modified Graphene Composite via One-Step Hydrothermal Method, *J. Electron. Mater.*, 2016, **45**, 4324–4330, DOI: 10.1007/s11664-016-4600-8.

123 Z. Liu, L. Yu, F. Guo, S. Liu, L. Qi, M. Shan and X. Fan, Facial development of high performance room temperature NO2 gas sensors based on ZnO nanowalls decorated rGO nanosheets, *Appl. Surf. Sci.*, 2017, **423**, 721–727, DOI: 10.1016/J.APSUSC.2017.06.160.

124 M. Bao, Y. Chen, F. Li, J. Ma, T. Lv, Y. Tang, L. Chen, Z. Xu and T. Wang, Plate-like p-n heterogeneous NiO/WO3 nanocomposites for high performance room temperature NO2 sensors, *Nanoscale*, 2014, **6**, 4063–4066, DOI: 10.1039/c3nr05268k.

125 T. Wang, J. Hao, S. Zheng, Q. Sun, D. Zhang and Y. Wang, Highly sensitive and rapidly responding room-temperature NO2 gas sensors based on WO3 nanorods/sulfonated graphene nanocomposites, *Nano Res.*, 2018, **11**, 791–803, DOI: 10.1007/s12274-017-1688-y.

126 J. Zhang, Z. Qin, D. Zeng and C. Xie, Metal-oxide-semiconductor based gas sensors: Screening, preparation, and integration, *Phys. Chem. Chem. Phys.*, 2017, **19**, 6313–6329, DOI: 10.1039/c6cp07799d.

127 S. Liu, Z. Wang, Y. Zhang, J. Li and T. Zhang, Sulfonated graphene anchored with tin oxide nanoparticles for detection of nitrogen dioxide at room temperature with enhanced sensing performances, *Sens. Actuators, B*, 2016, **228**, 134–143, DOI: 10.1016/j.snb.2016.01.023.

128 Y. Xia, J. Wang, X. Li, D. Xie, D. Zhou, L. Xiang and S. Komarneni, Nanoseed-assisted rapid formation of ultrathin

ZnO nanorods for efficient room temperature NO2 detection, *Ceram. Int.*, 2016, **42**, 15876–15880, DOI: 10.1016/j.ceramint.2016.07.058.

129 Y. L. Dong, X. F. Zhang, X. L. Cheng, Y. M. Xu, S. Gao, H. Zhao and L. H. Huo, Highly selective NO2 sensor at room temperature based on nanocomposites of hierarchical nanosphere-like α-Fe2O3 and reduced graphene oxide, *RSC Adv.*, 2014, **4**, 57493–57500, DOI: 10.1039/c4ra10136g.

130 V. P. Verma, S. Das, S. Hwang, H. Choi, M. Jeon and W. Choi, Nitric oxide gas sensing at room temperature by functionalized single zinc oxide nanowire, *Mater. Sci. Eng. B: Solid-State Mater. Adv. Technol.*, 2010, **171**, 45–49, DOI: 10.1016/j.mseb.2010.03.066.

131 H. Xu, J. Zhang, A. U. Rehman, L. Gong, K. Kan, L. Li and K. Shi, Synthesis of NiO@CuO nanocomposite as high-performance gas sensing material for NO 2 at room temperature, *Appl. Surf. Sci.*, 2017, **412**, 230–237, DOI: 10.1016/j.apsusc.2017.03.213.

132 W. Fang, Y. Yang, H. Yu, X. Dong, R. Wang, T. Wang, J. Wang, Z. Liu, B. Zhao and X. Wang, An In2O3 nanorod-decorated reduced graphene oxide composite as a high-response NOx gas sensor at room temperature, *New J. Chem.*, 2017, **41**, 7517–7523, DOI: 10.1039/c7nj00993c.

133 Y. Wei, C. Chen, G. Yuan and S. Gao, SnO2 nanocrystals with abundant oxygen vacancies: Preparation and room temperature NO2 sensing, *J. Alloys Compd.*, 2016, **681**, 43–49, DOI: 10.1016/j.jallcom.2016.04.220.

134 S. Öztürk, N. Kilinç and Z. Z. Öztürk, Fabrication of ZnO nanorods for NO2 sensor applications: Effect of dimensions and electrode position, *J. Alloys Compd.*, 2013, **581**, 196–201, DOI: 10.1016/j.jallcom.2013.07.063.

135 Y. Yang, C. Tian, L. Sun, R. Lü, W. Zhou, K. Shi, K. Kan, J. Wang and H. Fu, Growth of small sized CeO2 particles in the interlayers of expanded graphite for high-performance room temperature NOx gas sensors, *J. Mater. Chem. A*, 2013, **1**, 12742–12749, DOI: 10.1039/c3ta12399e.

136 X. Mu, C. Chen, L. Han, B. Shao, Y. Wei, Q. Liu and P. Zhu, Indium oxide octahedrons based on sol-gel process enhance room temperature gas sensing performance, *J. Alloys Compd.*, 2015, **637**, 55–61, DOI: 10.1016/j.jallcom.2015.03.002.

137 T. Xie, N. Sullivan, K. Steffens, B. Wen, G. Liu, R. Debnath, A. Davydov, R. Gomez and A. Motayed, UV-assisted room-temperature chemiresistive NO2 sensor based on TiO2 thin film, *J. Alloys Compd.*, 2015, **653**, 255–259, DOI: 10.1016/j.jallcom.2015.09.021.

138 L.-Y. Hong and H.-N. Lin, NO gas sensing at room temperature using single titanium oxide nanodot sensors created by atomic force microscopy nanolithography, *Beilstein J. Nanotechnol.*, 2016, **7**, 1044–1051, DOI: 10.3762/bjnano.7.97.

139 Y. Yang, C. Tian, J. Wang, L. Sun, K. Shi, W. Zhou and H. Fu, Facile synthesis of novel 3D nanoflower-like CuxO/multilayer graphene composites for room temperature NOx gas sensor application, *Nanoscale*, 2014, **6**, 7369–7378, DOI: 10.1039/c4nr00196f.

140 Y. X. Li, Z. X. Song, F. Jiang, Q. Sun, F. Ma, H. R. Wang and K. Chen, Thermal annealing induced mazy structure on MoO3 thin films and their high sensing performance to NO gas at room temperature, *Ceram. Int.*, 2016, **42**, 18318–18323, DOI: 10.1016/j.ceramint.2016.08.162.

141 R. Lü, W. Zhou, K. Shi, Y. Yang, L. Wang, K. Pan, C. Tian, Z. Ren and H. Fu, Alumina decorated TiO2 nanotubes with ordered mesoporous walls as high sensitivity NOx gas sensors at room temperature, *Nanoscale*, 2013, **5**, 8569–8576, DOI: 10.1039/c3nr01903a.

142 X. Geng, C. Zhang, Y. Luo and M. Debliquy, Flexible NO2 gas sensors based on sheet-like hierarchical ZnO1−x coatings deposited on polypropylene papers by suspension flame spraying, *J. Taiwan Inst. Chem. Eng.*, 2017, **75**, 280–286, DOI: 10.1016/j.jtice.2017.03.021.

143 U. Yaqoob, D. T. Phan, A. S. M. I. Uddin and G. S. Chung, Highly flexible room temperature NO2 sensor based on MWCNTs-WO3 nanoparticles hybrid on a PET substrate, *Sens. Actuators, B*, 2015, **221**, 760–768, DOI: 10.1016/j.snb.2015.06.137.

144 S. J. Choi, H. J. Choi, W. T. Koo, D. Huh, H. Lee and I. D. Kim, Metal-Organic Framework-Templated PdO-Co3O4 Nanocubes Functionalized by SWCNTs: Improved NO2 Reaction Kinetics on Flexible Heating Film, *ACS Appl. Mater. Interfaces*, 2017, **9**, 40593–40603, DOI: 10.1021/acsami.7b11317.

145 C. Y. Lee, S. J. Kim, I. S. Hwang and J. H. Lee, Glucose-mediated hydrothermal synthesis and gas sensing characteristics of WO3 hollow microspheres, *Sens. Actuators, B*, 2009, **142**, 236–242, DOI: 10.1016/j.snb.2009.08.031.

146 A. U. Rehman, J. Zhang, J. Zhou, K. Kan, L. Li and K. Shi, Synthesis of mesoporous K2O-In2O3 nanowires and NOx gas sensitive performance study in room temperature, *Microporous Mesoporous Mater.*, 2017, **240**, 50–56, DOI: 10.1016/j.micromeso.2016.11.006.

147 H. Zhang, L. Yu, Q. Li, Y. Du and S. Ruan, Reduced graphene oxide/α-Fe2O3 hybrid nanocomposites for room temperature NO2 sensing, *Sens. Actuators, B*, 2017, **241**, 109–115, DOI: 10.1016/j.snb.2016.10.059.

148 J. Pan, W. Liu, L. Quan, N. Han, S. Bai, R. Luo, Y. Feng, D. Li and A. Chen, Cu2O and rGO Hybridizing for Enhancement of Low-Concentration NO2 Sensing at Room Temperature, *Ind. Eng. Chem. Res.*, 2018, **57**, 10086–10094, DOI: 10.1021/acs.iecr.8b01430.

149 L. Meng, Q. Xu, Z. Sun, G. Li, S. Bai, Z. Wang and Y. Qin, Enhancing the performance of room temperature ZnO microwire gas sensor through a combined technology of surface etching and UV illumination, *Mater. Lett.*, 2018, **212**, 296–298, DOI: 10.1016/j.matlet.2017.10.102.

150 X. Liu, J. Sun and X. Zhang, Novel 3D graphene aerogel-ZnO composites as efficient detection for NO2 at room temperature, *Sens. Actuators, B*, 2015, **211**, 220–226, DOI: 10.1016/j.snb.2015.01.083.

151 N. Chen, X. Li, X. Wang, J. Yu, J. Wang, Z. Tang and S. A. Akbar, Enhanced room temperature sensing of Co3O4-

intercalated reduced graphene oxide based gas sensors, *Sens. Actuators, B*, 2013, **188**, 902–908, DOI: 10.1016/j. snb.2013.08.004.

152 R. Gao, Z. Ying, W. Sheng and P. Zheng, Gas sensors based on ZnO/silk fibroin film for nitrogen dioxide detection under UV light at room temperature, *Mater. Lett.*, 2018, **229**, 210–212, DOI: 10.1016/j.matlet.2018.07.018.

153 F. Gu, R. Nie, D. Han and Z. Wang, In2O3-graphene nanocomposite based gas sensor for selective detection of NO2 at room temperature, *Sens. Actuators, B*, 2015, **219**, 94–99, DOI: 10.1016/j.snb.2015.04.119.

154 V. Srivastava and K. Jain, At room temperature graphene/ SnO2 is better than MWCNT/SnO2 as NO2 gas sensor, *Mater. Lett.*, 2016, **169**, 28–32, DOI: 10.1016/j. matlet.2015.12.115.

155 S. Maeng, S. W. Kim, D. H. Lee, S. E. Moon, K. C. Kim and A. Maiti, SnO2 nanoslab as NO2 sensor: Identification of the NO2 sensing mechanism on a SnO2 surface, *ACS Appl. Mater. Interfaces*, 2014, **6**, 357–363, DOI: 10.1021/ am404397f.

156 U. Yaqoob, A. S. M. I. Uddin and G. S. Chung, A high-performance flexible NO2 sensor based on WO3 NPs decorated on MWCNTs and RGO hybrids on PI/PET substrates, *Sens. Actuators, B*, 2016, **224**, 738–746, DOI: 10.1016/j.snb.2015.10.088.

157 N. D. Chinh, N. D. Quang, H. Lee, T. T. Hien, N. M. Hieu, D. Kim, C. Kim and D. Kim, NO gas sensing kinetics at room temperature under UV light irradiation of In2 O3 nanostructures, *Sci. Rep.*, 2016, **6**, 1–11, DOI: 10.1038/srep35066.

158 A. J. Thomson, G. Giannopoulos, J. Pretty, E. M. Baggs and D. J. Richardson, Biological sources and sinks of nitrous oxide and strategies to mitigate emissions, *Philos. Trans. R. Soc., B*, 2012, **367**, 1157–1168, DOI: 10.1098/rstb.2011.0415.

159 L. Valentini, I. Armentano, J. M. Kenny, C. Cantalini, L. Lozzi and S. Santucci, Sensors for sub-ppm NO2 gas detection based on carbon nanotube thin films, *Appl. Phys. Lett.*, 2003, **82**, 961–963, DOI: 10.1063/1.1545166.

160 X. Jiang, H. Tai, Z. Ye, Z. Yuan, C. Liu, Y. Su and Y. Jiang, Novel p-n heterojunction-type rGO/CeO2 bilayer membrane for room-temperature nitrogen dioxide detection, *Mater. Lett.*, 2017, **186**, 49–52, DOI: 10.1016/j.matlet.2016.08.010.

161 X. Liu, J. Li, J. Sun and X. Zhang, 3D Fe3O4 nanoparticle/ graphene aerogel for NO2 sensing at room temperature, *RSC Adv.*, 2015, **5**, 73699–73704, DOI: 10.1039/c5ra14857j.

162 Y. Xia, J. Wang, J. L. Xu, X. Li, D. Xie, L. Xiang and S. Komarneni, Confined Formation of Ultrathin ZnO Nanorods/Reduced Graphene Oxide Mesoporous Nanocomposites for High-Performance Room-Temperature NO2 Sensors, *ACS Appl. Mater. Interfaces*, 2016, **8**, 35454–35463, DOI: 10.1021/acsami.6b12501.

163 P. G. Su and T. T. Pan, Fabrication of a room-temperature NO2 gas sensor based on WO3 films and WO3/MWCNT nanocomposite films by combining polyol process with metal organic decomposition method, *Mater. Chem. Phys.*, 2011, **125**, 351–357, DOI: 10.1016/j. matchemphys.2010.11.001.

164 K. K. Sadasivuni, D. Ponnamma, H. U. Ko, H. C. Kim, L. Zhai and J. Kim, Flexible NO2 sensors from renewable cellulose nanocrystals/iron oxide composites, *Sens. Actuators, B*, 2016, **233**, 633–638, DOI: 10.1016/j. snb.2016.04.134.

165 V. Annapureddy, Y. Kim, G.-T. Hwang, H. W. Jang, S.-D. Kim, J.-J. Choi, B. Cho and J. Ryu, Flexible Gas Sensors: Room-Temperature Solid-State Grown WO 3−δ Film on Plastic Substrate for Extremely Sensitive Flexible NO 2 Gas Sensors (Adv. Mater. Interfaces 1/2018), *Adv. Mater. Interfaces*, 2018, **5**, 1870001, DOI: 10.1002/ admi.201870001.

166 Z. Bo, X. Wei, X. Guo, H. Yang, S. Mao, J. Yan and K. Cen, SnO2 nanoparticles incorporated CuO nanopetals on graphene for high-performance room-temperature NO2 sensor, *Chem. Phys. Lett.*, 2020, **750**, 137485, DOI: 10.1016/j. cplett.2020.137485.

167 S. S. Sangale, V. V. Jadhav, S. F. Shaikh, P. V. Shinde, B. G. Ghule, S. D. Raut, M. S. Tamboli, A. M. Al-Enizi and R. S. Mane, Facile one-step hydrothermal synthesis and room-temperature NO2 sensing application of α-Fe2O3 sensor, *Mater. Chem. Phys.*, 2020, **246**, 122799, DOI: 10.1016/j. matchemphys.2020.122799.

168 D. Chavez, C. Gomez-Solis, A. I. Mtz-Enriquez, V. Rodriguez-Gonzalez, V. Escobar-Barrios, C. R. Garcia and J. Oliva, High sensitivity of flexible graphene composites decorated with V2O5 microbelts for NO2 detection, *Mater. Res. Bull.*, 2021, **133**, 111052, DOI: 10.1016/j. materresbull.2020.111052.

169 Y.-H. Zhang, C.-N. Wang, L.-J. Yue, J.-L. Chen, F.-L. Gong and S.-M. Fang, Nitrogen-doped graphene quantum dot decorated ultra-thin ZnO nanosheets for NO2 sensing at low temperatures, *Phys. E*, 2021, **133**, 114807, DOI: 10.1016/ j.physe.2021.114807.

170 N. M. Hung, C. M. Hung, N. Van Duy, N. D. Hoa, H. S. Hong, T. K. Dang, N. N. Viet, L. V. Thong, P. H. Phuoc and N. Van Hieu, Significantly enhanced NO2 gas-sensing performance of nanojunction-networked SnO2 nanowires by pulsed UV-radiation, *Sens. Actuators, A*, 2021, **327**, 112759, DOI: 10.1016/j.sna.2021.112759.

171 T. H. Han, S. Y. Bak, S. Kim, S. H. Lee, Y. J. Han and M. Yi, Decoration of cuo nws gas sensor with zno nps for improving no2 sensing characteristics, *Sensors*, 2021, **21**, 1–11, DOI: 10.3390/s21062103.

172 X. Chen, S. Wang, C. Su, Y. Han, C. Zou, M. Zeng, N. Hu, Y. Su, Z. Zhou and Z. Yang, Two-dimensional Cd-doped porous Co3O4 nanosheets for enhanced room-temperature NO2 sensing performance, *Sens. Actuators, B*, 2020, **305**, 127393, DOI: 10.1016/j.snb.2019.127393.

173 B. Sharma, A. Sharma and J. H. Myung, Selective ppb-level NO2 gas sensor based on SnO2-boron nitride nanotubes, *Sens. Actuators, B*, 2021, **331**, 129464, DOI: 10.1016/j. snb.2021.129464.

174 N. M. Hung, C. M. Hung, N. Van Duy, N. D. Hoa, H. S. Hong, T. K. Dang, N. N. Viet, L. V. Thong, P. H. Phuoc and N. Van Hieu, Significantly enhanced NO2 gas-sensing

performance of nanojunction-networked SnO2 nanowires by pulsed UV-radiation, *Sens. Actuators, A*, 2021, **327**, 112759, DOI: 10.1016/j.sna.2021.112759.

175 R. Kumar, O. Al-Dossary, G. Kumar and A. Umar, Zinc oxide nanostructures for no2 gas–sensor applications: A review, *Nano-Micro Lett.*, 2015, **7**, 97–120, DOI: 10.1007/S40820-014-0023-3/FIGURES/1.

176 P. Rai, Y. S. Kim, H. M. Song, M. K. Song and Y. T. Yu, The role of gold catalyst on the sensing behavior of ZnO

nanorods for CO and NO2 gases, *Sens. Actuators, B*, 2012, **1**, 133–142, DOI: 10.1016/J.SNB.2012.02.030.

177 T. J. Hsueh and S. S. Wu, Highly sensitive Co3O4 nanoparticles/MEMS NO2 gas sensor with the adsorption of the Au nanoparticles, *Sens. Actuators, B*, 2021, **329**, 129201, DOI: 10.1016/J.SNB.2020.129201.

178 R. Prajesh, N. Jain, V. K. Khanna, V. Gupta and A. Agarwal, MEMS based integrated gas sensor for NO2 and NH3, *Journal of ISSS*, 2014, **3**, 1–6.